System tests of the new electronics for the Central Fiber Tracker and Preshower detectors

J. Estrada, C. García, B. Hoeneisen and P. Rubinov

DØ note 4233,
15 August 2003

Abstract

We present system tests of 224 channels of the new electronics for the Central Fiber Tracker and Preshower detectors. We also compare the performance of the present electronics with the new electronics to help make the decision of wether to replace it or not. At present the tracking efficiency at $\eta = 0$ is $\approx 70\%$ due to the low light yield of wide angle tracks. With the present electronics this efficiency is expected to drop to $\approx 39\%$ at the end of Run II due to fiber aging and reduced gain of VLPC's at high background rates. Also combinatoric background will become overwhelming at a luminosity above $\approx 100 \cdot 10^{30} \mathrm{cm}^{-2}\mathrm{s}^{-1}$ (at a benchmark tracking performance). The new electronics will increase the tracking efficiency at $\eta = 0$ at the end of Run II to $\approx 87\%$ and will increase the luminosity (at which the same benchmark tracking performance is met) to $\approx 200 \cdot 10^{30} \mathrm{cm}^{-2}\mathrm{s}^{-1}$.

1 Introduction

We present system tests of 224 channels of the new electronics for the Central Fiber Tracker (CFT) and Preshower detectors. We also compare the performance of the present electronics with the new electronics to help make the decision of wether to replace it or not.

For the benefit of the reader unfamiliar with this project we briefly summarize its history. The original plan of operation of the Tevatron was to switch from 396ns bunch crossing in Run IIa to 132ns bunch crossing in Run IIb. The "SIFT" chips in the Multi Channel Modules (MCM's) in the Analog Front End boards (AFE's) of the Central Fiber Tracker (CFT) and Preshower detectors can not operate at 132ns bunch crossing.[1] For this reason a new

MCM with a new custom "TriP" chip was designed[2], built and tested.[3, 4] The first (and only) submission of the chip met all specifications[2] which is a mayor achievement by its designer Abderrezak Mekkaoui. Seven thousand chips are in-hand, enough to populate all new AFE's. However the current plan of the Tevatron is to abandon operation at 132ns bunch crossing. At 396ns bunch crossing the analog pipeline of the TriP chip is sufficiently deep to store the time at which the discriminators fire in addition to the amplitude of the pulses. This feature permits a coarse measurement of the z-coordinate in the CFT after the L1 trigger accept. This z-coordinate measurement effectively doubles the number of pixels in the CFT[5], reduces the combinatoric background of tracking, speeds up the tracking algorithm, and allows the CFT to operate at about twice the luminosity.[5] This added functionality of the TriP chip requires a new submission of the chip (TriP-t). The re-design effort is minor and of low risk since the silicon real estate is available, no circuits have to be moved, and no pins have to be reassigned. This re-design may be made in October. At present an AFE II board is being laid out and ten boards will be fabricated and tested before the end of 2003. TriP-t will require modifications of Firmware but not of the hardware on the AFE II. The AFE II boards are a transparent plugin replacement of the AFE I boards.

2 Test setup

We used a test stand on the 3rd floor of the DØ Assembly Building. This test stand has a computer, a Stand-Alone-Sequencer, an AFE I on a Visible Photon Light Counter (VLPC) cryostat and cassette. The VLPC's are illuminated by pulsing Light Emitting Diodes in synchronism with the TURN_START signal. Modules 0 and 1 of the AFE I board have MCM IIb's with two bare TriP chips; module 2 has an MCM IIb with one working bare TriP chip; module 3 has an MCM IIc with one encapsulated TriP chip; and module 5 has an MCM IIc with one bare TriP chip. In total we tested all 224 channels of the 7 TriP chips (except for a few channels that have no VLPC bias in this AFE for reasons we did not investigate). The values of the TriP chip registers used for these measurements are presented in Table 1, except for the time scans for which the threshold is set at R10 = 210. The meaning of the registers is defined in [3].

R1	R2	R3	R4	R5	R6	R7	R8	R9	R10	R11	R12
130	120	20	160	138	24	42	10	155	218	479	479

Table 1: Registers in TriP chips. See [3] for a description of the registers.

3 Firmware

The firmware of the FPGA on the MCM's for operation at 396ns bunch crossing can be found in D0server6 $\rightarrow$ projects $\rightarrow$ TriggerElectronics $\rightarrow$ 396ns in files MCMIIB_396_30JUL2003.ZIP and MCMIIC_396_30JUL2003.ZIP. The MCM has 4 modes of operation controlled by the lines MOD0, MOD1 and CHANGE_MODE as explained in [2]: INITIALIZE, ACQUIRE, DIGITIZE and READOUT. Normal data taking occurs in ACQUIRE mode. Upon receiving an L1 trigger (SKIPB signal) the MCM goes into DIGITIZE and READOUT modes. The controls from the Sequencer are the same as with the present electronics. The clocks are shown in Figures 1 and 2. The MCM receives two external clocks: CLK_30 synchronous with beam crossing (of 33ns period) and TURN_START. The downward transition of TURN_START in the beam gap synchronizes the 396ns period. In addition the MCM receives the SVX_CLK in READOUT mode. The READOUT is by Daisy Chain controlled by the Sequencer with signals PRIORITY_IN and PRIORITY_OUT and is clocked from the active FPGA in the Daisy Chain using DVALID.

The window of integration of charge was chosen to be 82.5ns (but may be set to other values if required), see Figures 3 and 4.

We propose having two sets of firmware: one reads out 8 ADC bits for light spectra studies, and one reads out 4 bits of ADC and 4 bits of TDC for data acquisition with a coarse z measurement using the time-of-flight.

The TriP chip preamplifyer has two gain settings and the opamp for the analog signal has 8 gain settings to acomodate the dynamic ranges needed by the CFT and the Preshower detectors.

4 Results

The results of the measurements are shown in Figures 5 through 40. Figure 5 shows the analog output of the TriP chip as a function of injected charge. The slope is 2.244 ADC counts per fC. Figure 6 shows the light spectrum and the discriminator turn on curve as a function of ADC. This turn-on curve shows all system effects as it is the ratio of the light spectrums with and without requiring discriminator firing, *e.g.* light guides, VLPC gain,

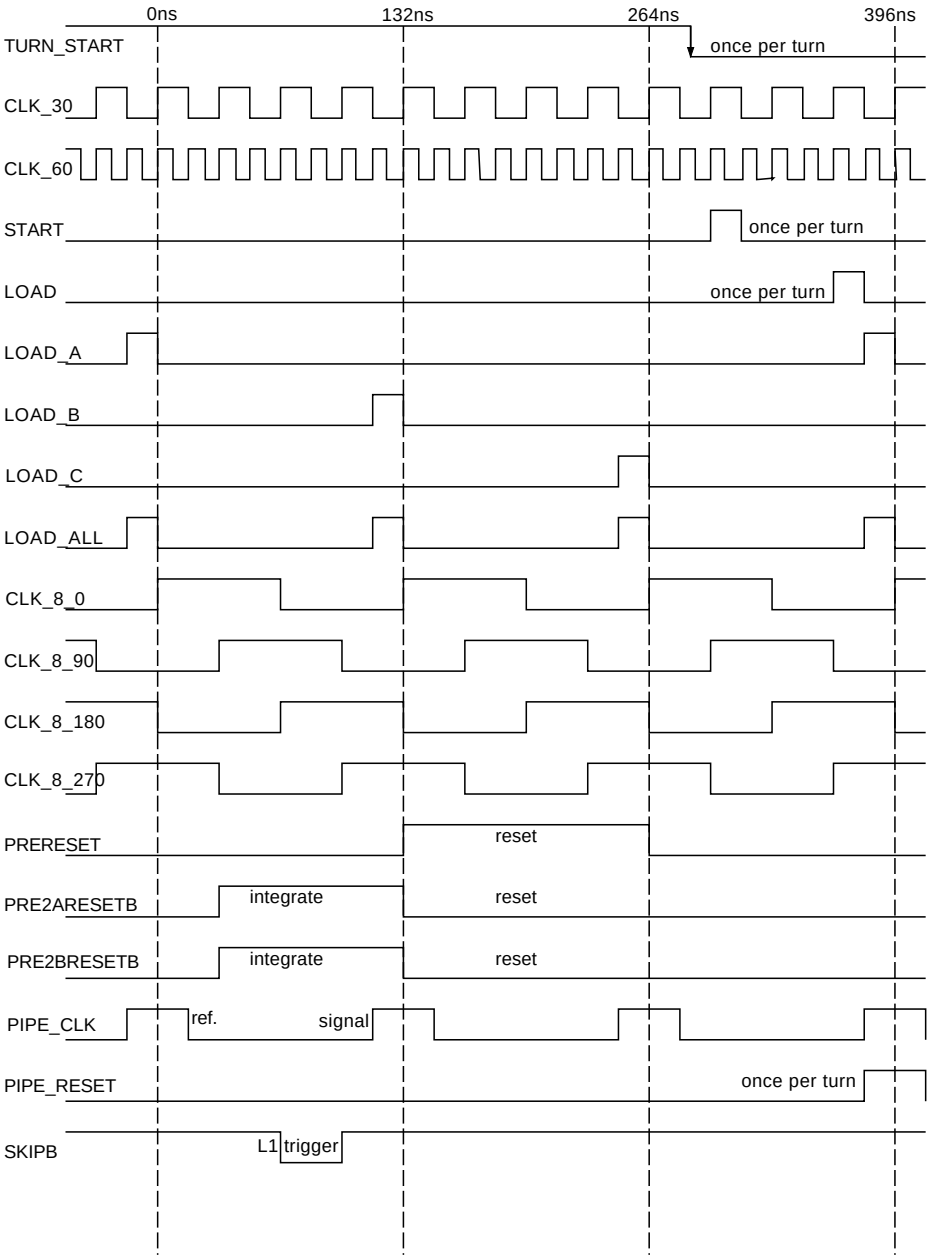

Figure 1: Clocks in the MCM FPGA for operation at 396ns bunch crossing.

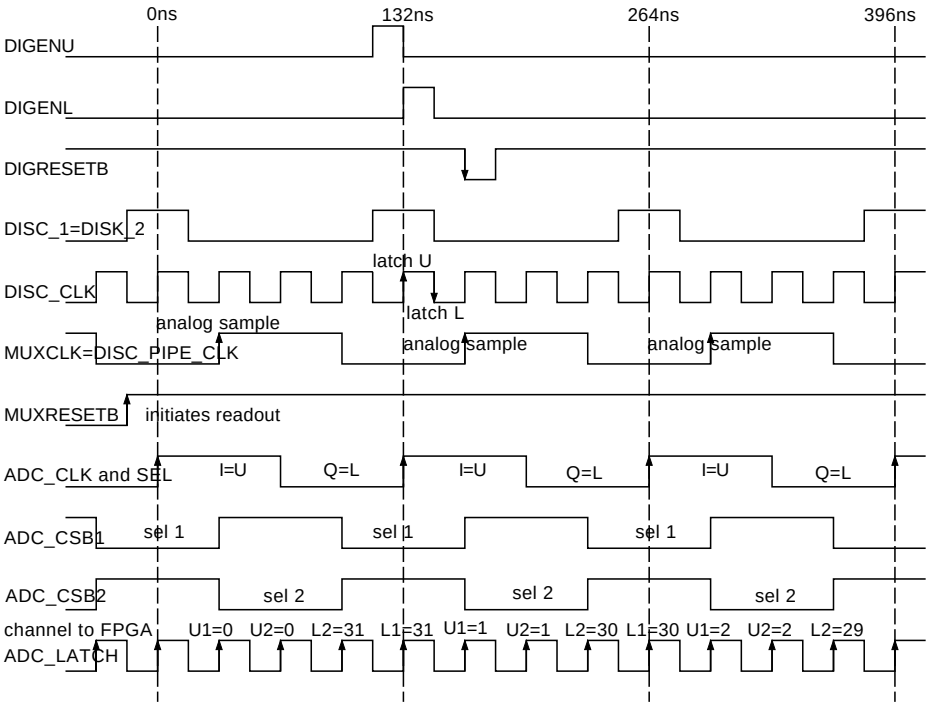

Figure 2: Continuation of Figure 1.

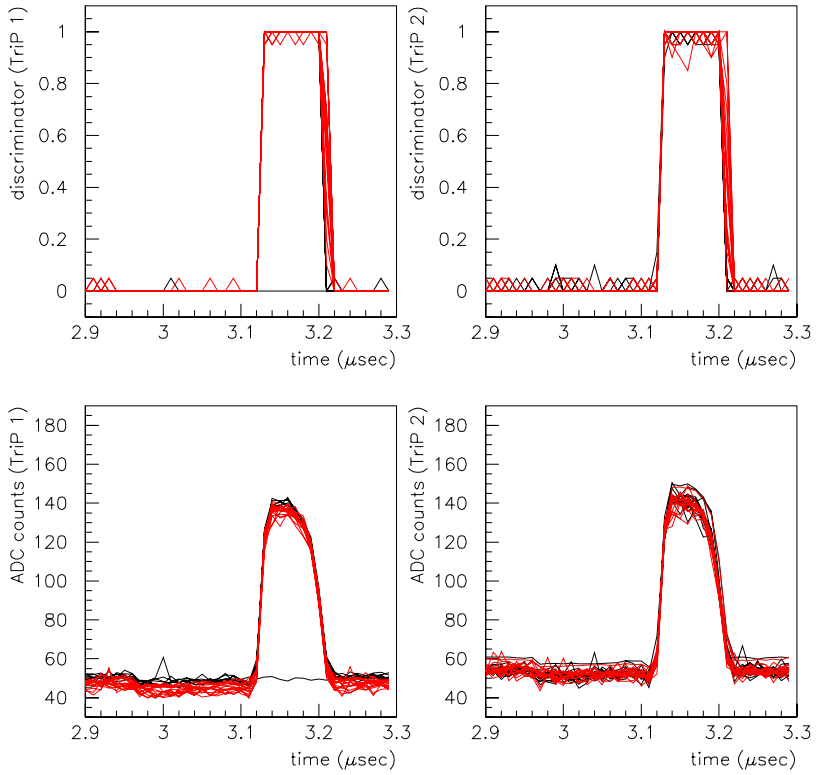

Figure 3: Window for charge integration for discriminator firing and analog output. 64 channels of Module 0. Programing of the charge injection capacitor does not work for 1 channel, tho the channel is otherwise OK. The TriP was tested stand-alone and the programming for it is OK.

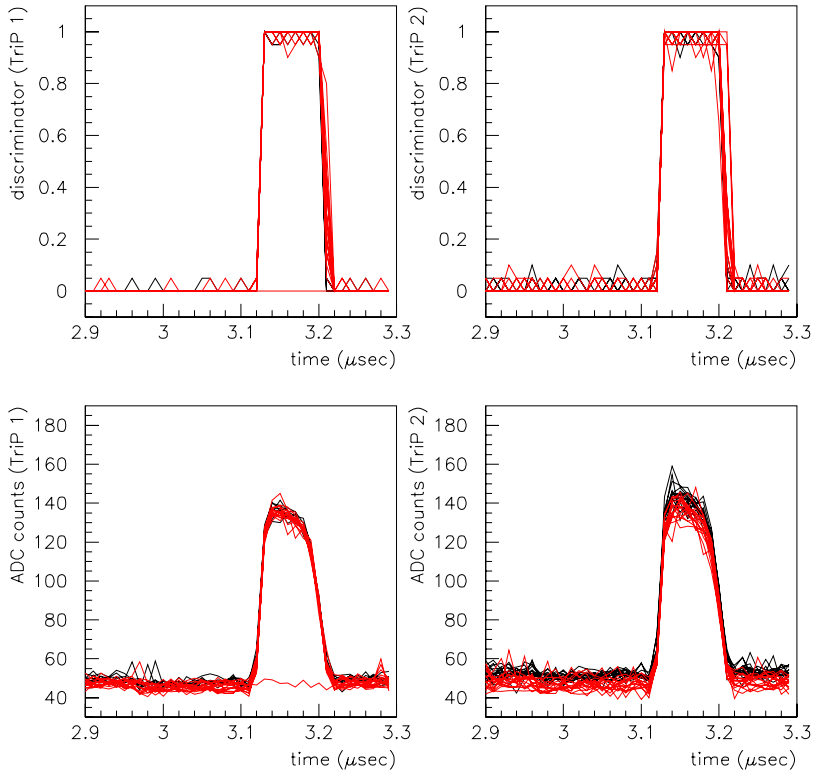

Figure 4: Window for charge integration for discriminator firing and analog output. 64 channels of Module 1. Programing of the charge injection capacitor does not work for 1 channel, tho the channel is otherwise OK. The TriP was tested stand-alone and the programming for it is OK.

flex cable capacitance and any pickups due to switching digital lines and circuit layout of analog inputs up to the TriP chips. [1] Figure 7 shows the discriminator turn-on curves of the 64 channels of MCM IIb at module 0. Some noise is observed before turn on in some channels which is peculiar to MCM IIb and not MCM IIc (compare Figures 7, 14, 21, 28 and 35). Figure 8 shows the discriminator turn on curves as a function of the number of photo-electrons obtained from the fit (for a few channels the fit did not converge even tho the spectra looks OK and for some channels the VLPC's have no bias for reasons we did not investigate).

The pedestal, gain, noise and mean obtained from the fits for the 64 channels of MCM IIb at module 0 are shown in Figures 9 and 10. In Figure 9 we observe that the first 5 channels of TriP 1 have high pedestals. This problem was already studies in [4]: it is due to cross-talk between digital lines and analog inputs to the TriP 1 chip. This problem does not appear for TriP 2 and will be avoided in the layout of AFE II which does not have the constraints of the MCM pins (since AFE II will have no MCM's). We studied this cross talk and found that it is due to the signals PRERESET, PRE2ARESETB and PRE2BRESETB: when these signals are removed the pedestal shift disappears.

In Figures 11 and 12 are shown the discriminator threshold (at which the probability of firing is 50%) and the discriminator width (half the interval from 16% and 84% firing), and their histograms. Let us compare the histograms in Figures 12, 19, 26, 33 and 40. The **full** spread among all channels (except the first 5 channels of TriP 1 as mentioned above) of the discriminator pedestals is 10, 10, 10, 12 and 6 ADC counts for modules 0, 1, 2 (which are MCM IIb's with bare TriP's), 3 (MCM IIc with packaged TriP) and 5 (MCM IIc with bare TriP) respectively. These numbers should be compared with the gain which varies from 10 to 20 ADC counts per photo-electron for the VLPC's in this cryostat (at 2.244 ADC counts per fC). Let us consider MCM IIc with the packaged TriP chip and an average VLPC gain (of 15 ADC counts per photoelectron). We set the threshold (pedestal) averaged over all channels at $12/(2 \cdot 15) + 3 \cdot 0.2 = 1.0$ photo-electrons, where 0.2 is the noise. Then even the worst channel is 3 "widths" (standard deviations) above the pedestal.

[1] The "easy" way to obtain discriminator turn-on curves is to inject charge directly into the TriP chip as was done in [4]. Here we have chosen the method of dividing histograms in order to tests the entire system. This method is sensitive to the convergence of the fit.

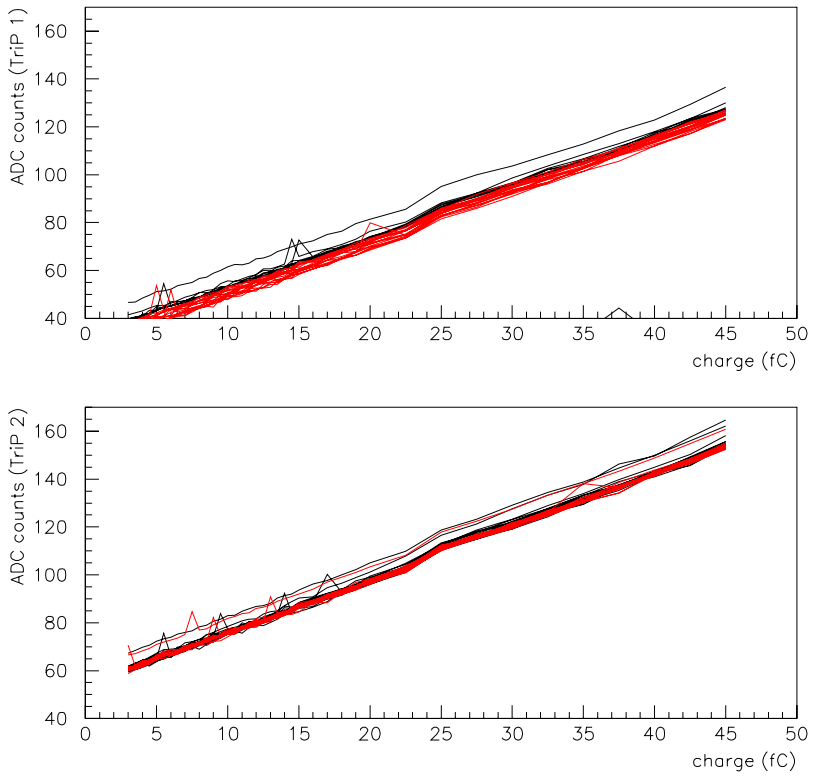

Figure 5: Analog output of the TriP chip in ADC counts *vs* injected charge. The slope is 2.244 ADC counts per fC. 64 channels of TriP 1 and 2, MCMIIb, module 0.

VLPC bias	window	noise from fit
off	82.5ns	1.207fC
on	82.5ns	1.451fC
off	57.75ns	1.116fC
on	57.75ns	1.609fC

Table 2: Noise obtained from gaussian fit (1 standard deviation) and rms noise. From data in Figures 43 to 46. To distinguish electronic noise and (electronic+VLPC dark current) noise we show the data without and with VLPC bias. Noise for 82.5ns and 57.75ns charge integration windows is shown.

5 Noise

The results of noise measurements are shown in Figures 41 to 46 without and with VLPC bias and with windows of charge integration of 82.5ns and 57.75ns (corresponding to the firmware for 396ns and 132ns bunch crossing respectively). The summary of these measurements is presented in Table 2. Our conclusion is that the electronic charge noise (1 standard deviation from the gaussian fit) of the TriP chip with associated circuits (35pF, 20ohm high density flex cable, 100K bias resistor, 100pF coupling capacitor) is

$$\Delta q_{rms} \approx 1.21 \text{ fC} \approx 7550 \text{ electrons} \quad (1)$$

for a window of integration of 82.5ns. To acomodate the requirements of the Central Fiber Tracker and the Preshower detectors we specified a large dynamic range for the chip in exchange for noise performance. Both specifications were met.[2]

6 Conclusions

We have presented system measurements of the performance of the new electronics for the Central Fiber Tracker and Preshower detectors for operation at 396ns bunch crossing. The first (and only) submission of the TriP chip and MCM II meet all specifications.[2] In order to decide wether to replace the existing electronics with the new one we compare their performances in Table 3.

The present electronics has ADC and mean discriminator thresholds ≈ 3.0 photo-electrons due to "split pedestals" and pedestal variations from bunch crossing to bunch crossing (the threshold distribution extends from 2.2 to 4.1

photo-electrons after an offline cut of 1.4 photo-electrons). Note that with the new electronics the threshold (at 50% efficiency) can be lowered safely to 1.5 photo-electrons (with a spread from 1.1 to 1.9). The effect of this change of threshold on tracking efficiency is summarized in Table 4.

The light yield of the inner layer fibers is expected to drop by $\approx 10\%$ after accumulating 6fb^{-1} of integrated luminosity (for light traversing half the fiber length).[7]

Let us now consider the gain of the VLPC's as a function of the background rate. As the background rate increases the VLPC gain drops.[6] This effect becomes more pronounced at higher VLPC bias voltage. From Figure 1 of [6] we observe that we must operate the VLPC's at typically > 6.8V in order to be fully efficient. At a CFT occupancy of 20% the background rate is $\approx 0.2 \cdot 8\text{pe}/396\text{ns} \approx 4\text{MHz}$ and the corresponding drop in gain is $\approx 16\%$ based on the measurements in Lab 3, see Figure 2 of [6]. The impact of this gain reduction is equivalent to raising the threshold by $\approx 16\%$.

Let us do a back-of-the-envelope calculation to estimate the importance of the fiber aging and VLPC background rate. In Figure 47 we show the present measured tracking efficiency for isolated high-p_T muons from $Z \to \mu^+\mu^-$. We note that at $\eta = 0$ the tracking efficiency drops due to low light yield to $\approx 70\%$.[8] As seen in Table 4, the corresponding number of photo-electrons is 8.4. Due to aging this number of photo-electrons is expected to drop by 10% and due to the VLPC background rate the threshold is expected to increase by 16%. Then the tracking efficiency at $\eta = 0$ will drop from $\approx 70\%$ to $\approx 39\%$ due to these two effects with the present electronics. For the new electronics the corresponding efficiencies are $\approx 97\%$ and $\approx 87\%$ respectively.

Now consider adding functionality to the TriP chip to measure the time at which the discriminators fire. This is a minor modification of the design of the TriP chip: the silicon real estate is available and the pipeline is sufficiently deep at 396ns bunch crossing to contain both the ADC and timing information. The measured[5] resolution is

$$\Delta z_{rms} = 46\sqrt{\frac{n}{8}}\text{cm} \tag{2}$$

where n is the number of photo-electrons, and is determined by the statistics of the photon arrival times. The time-of-flight measurement reduces the number of fake tracks at high occupancy and will permit extending the luminosity at which bench-mark tracking performance is achieved from $\approx 100 \cdot 10^{30}\text{cm}^{-2}\text{s}^{-1}$ to $\approx 200 \cdot 10^{30}\text{cm}^{-2}\text{s}^{-1}$.[5] Adding the timing measurement is equivalent to approximately doubling the number of pixels of the CFT at L3 and offline.

	AFE I	TriP	TriP-t
average ADC threshold	3.0pe*	1.5pe	1.5pe
average discriminator threshold	3.0pe	1.5pe	1.5pe
rms error on z coordinate	n.a.	n.a	46cm at center 27cm at ends of fiber

Table 3: Comparison between the present electronics (AFE I) and the new electronics using the TriP or TriP-t chips. TriP-t has added functionality to measure the time at which the discriminators fire.[5] *The threshold distribution extends from 2.2 to 4.1 photo-electrons after an offline cut of 1.4 photo-electrons. This cut is applied by choice to reduce combinatoric background so it is not clear if an advantage can be obtained with a lower threshold.

An additional advantage of the TriP chip is the reduced dead time for readout as discussed in [6]. This lower readout time is due to the abscence of the "virtual SVX". The readout time for 40% occupancy is reduced from 10.1ns to 7.7ns. Finally we mention that we are running out of spares for AFE I.

The cost of the new electronics is ≈\$500K and the lead time is ≈1.5 years. AFE II is mechanically and electrically compatible with the AFE I, so the Sequencer needs no changes. The replacement of the ≈ 200 AFE I boards should be transparent and not take more than about 2 days of collision hall access. Some unpaking code must be modified due to the new order in which the channels are read out.

References

[1] Paul Rubinov and Bruce Hoeneisen, DØ note 3897 (2001)

[2] P. Rubinov and B. Hoeneisen, DØ note 3898 (2001)

[3] J. Estrada, C. García, B. Hoeneisen, P. Rubinov, DØ note 4009 (2002)

[4] Juan Estrada, Charly García, Bruce Hoeneisen, Paul Rubinov, DØ note 4076 (2002)

[5] J. Estrada, C. Garcia, B. Hoeneisen and P. Rubinov, DØ note 4202 (2003)

[6] J. Estrada, M. Johnson and P. Rubinov, http://www-clued0.fnal.gov/ estrada/afeii.pdf, auxiliary file to this D0 note.

	AFE I	TriP	AFE I	TriP
light yield	doublet ϵ 3.0 pe thresh.	doublet ϵ 1.5 pe	tracking ϵ 3.0 pe	tracking ϵ 1.5 pe
12 pe	99.9%	100.0%	97.8%	99.9%
10 pe	99.3%	100.0%	90.0%	99.2%
9 pe	98.6%	99.9%	80.2%	98.0%
8 pe	97.2%	99.7%	63.4%	95.3%
7 pe	94.4%	99.3%	40.0%	88.9%
6 pe	89.3%	98.3%	16.5%	75.6%
5 pe	80.5%	96.0%	3.1%	51.7%

Table 4: Effect of the number of photo-electrons (pe) and threshold on the efficiency per fiber tracker doublet and per CFT track with 16 hits (a not unreasonable requirement at the high occupancies of Run IIb). Present (new) electronics has a threshold of 3.0 (1.5) photo-electrons.

[7] From Alan Bross (private communication): At 2fb^{-1} (6fb^{-1}) the dose is 10Krad (30Krad) in the inner layer of the CFT and the corresponding light yield drop is 10% (20%) for 2.5m of fiber.

[8] "Z $\rightarrow \mu^+\mu^-$ Cross Section", Emily Nurse, Physics Marathon for LP03, in D0 Agenda Server $\rightarrow$ Workshops, (2003).

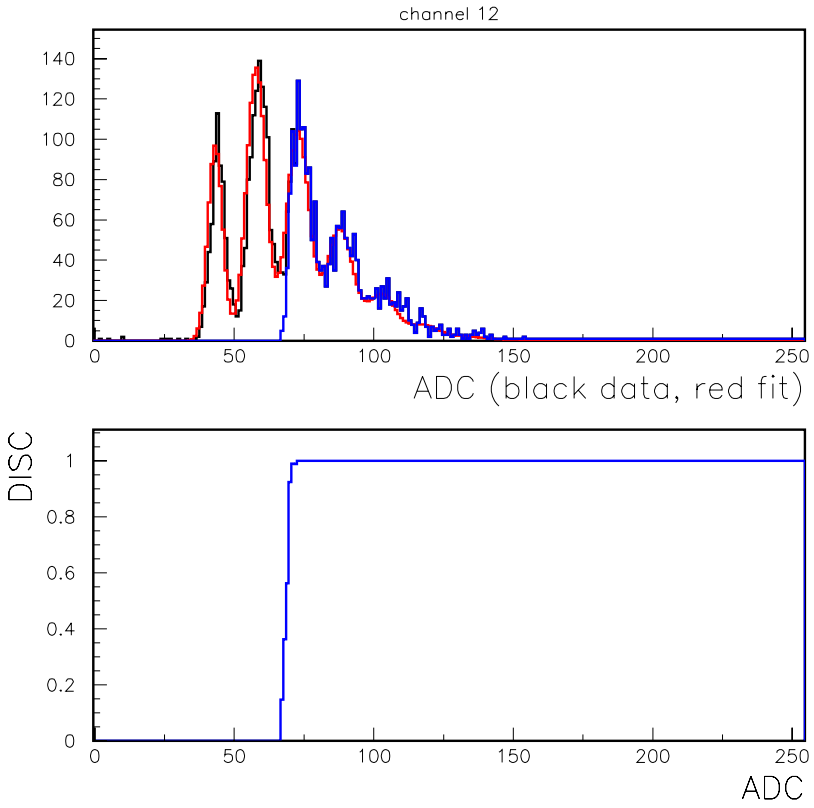

Figure 6: Histogram of ADC for all events and for events with discriminator fired (upper plot) and their ratio (lower plot). Also shown in the upper plot is the fit used to extract pedestal, gain, noise and mean number of photo-electrons. The peaks correspond to 0, 1, 2, 3 and 4 photo-electrons. Channel 12, TriP 1, MCM IIb, Module 0.

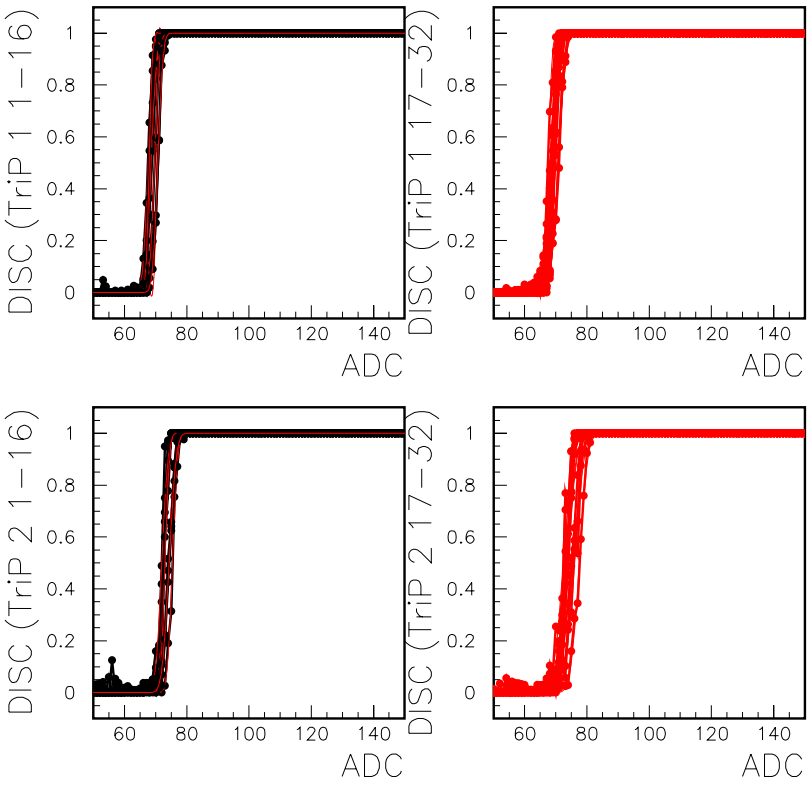

Figure 7: Discriminator turn-on curves for 64 channels as a function of ADC count (as in the lower plot of Figure 6). TriP 1 and 2, MCM IIb, Module 0.

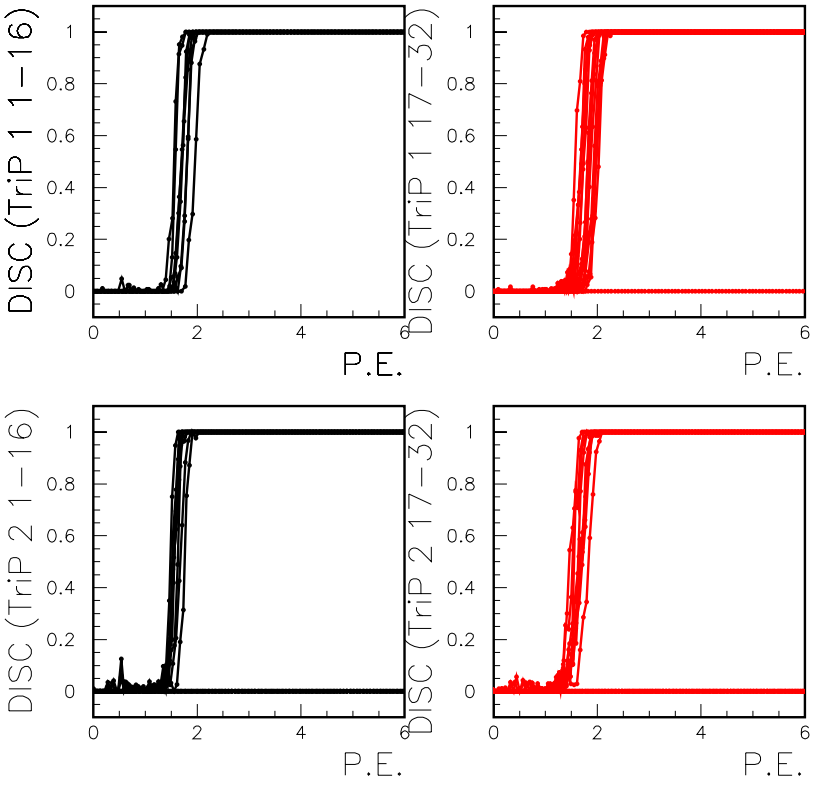

Figure 8: Discriminator turn-on curves for 64 channels as a function of the number of photo-electrons obtained from the fit. The fit did not converge for a few channels. TriP 1 and 2, MCM IIb, Module 0.

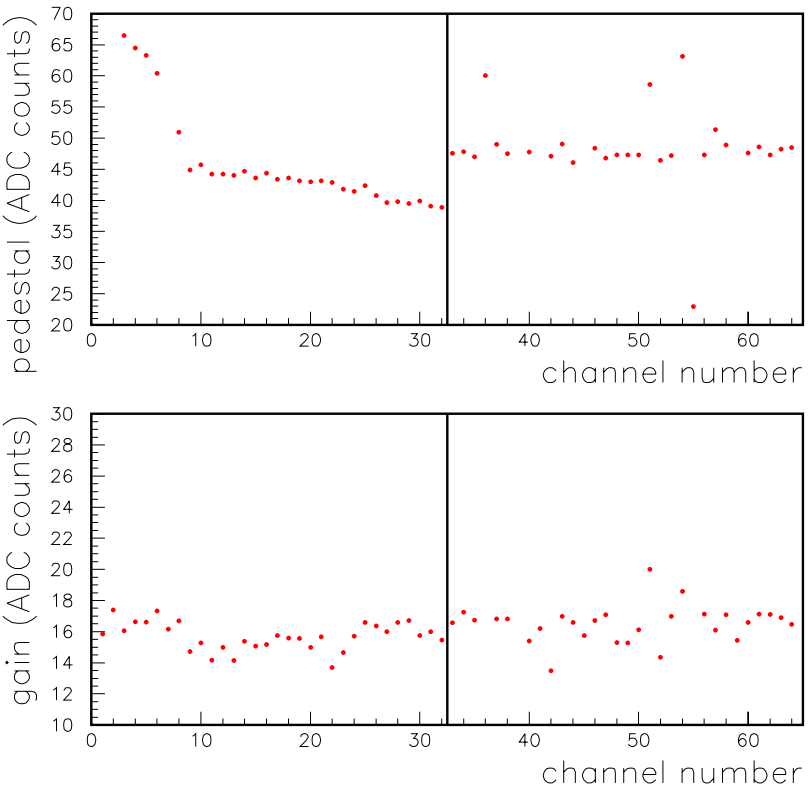

Figure 9: Pedestal and gain for 64 channels. TriP 1 and 2, MCM IIb, Module 0. The high pedestal of channels 1 to 5 of TriP 1 is due to cross-talk between digital clocks and analog inputs, which should be absent in AFE II, see the text.

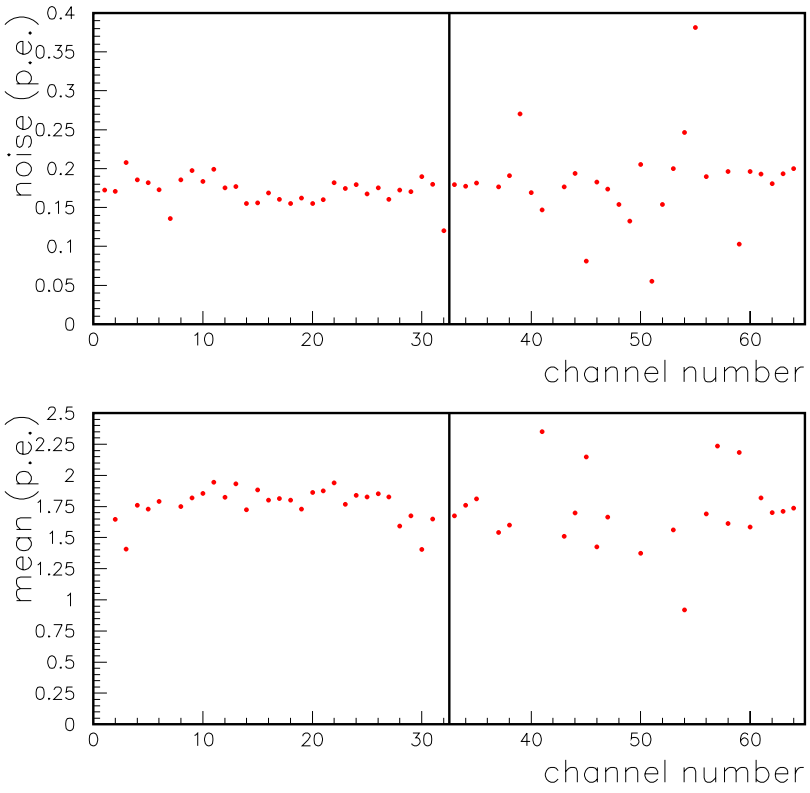

Figure 10: Noise (one standard deviation) and mean number of photo-electrons for 64 channels. TriP 1 and 2, MCM IIb, Module 0. Some fits are bad tho the spectra looks OK.

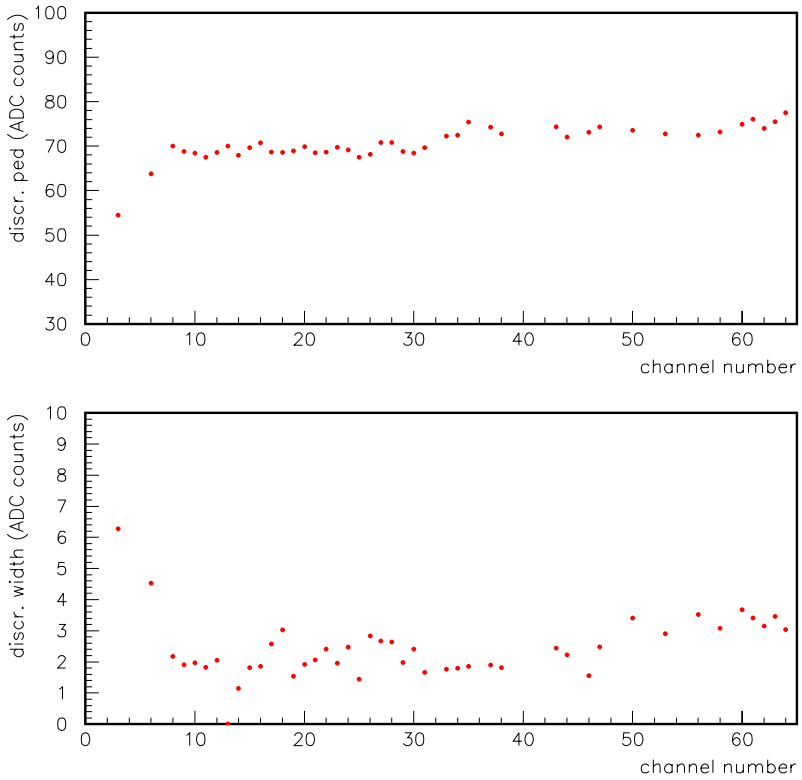

Figure 11: Discriminator pedestal (at which it fires 50% of the time) and discriminator width (1 standard deviation) for 64 channels. TriP 1 and 2, MCM IIb, Module 0. The discriminator width is half the interval from 16% firing to 84% firing as determined by the fitted error function.

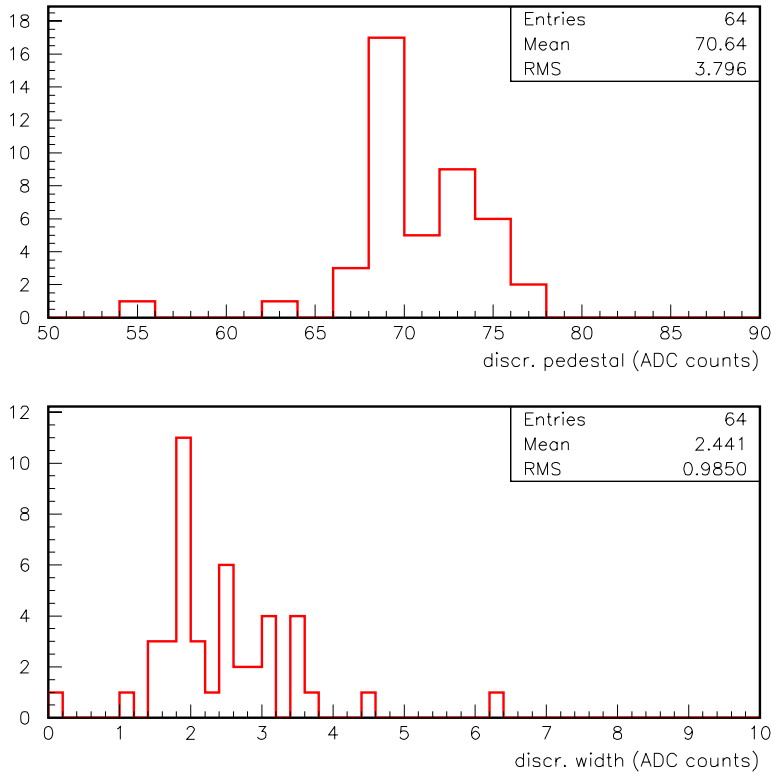

Figure 12: Histogram of discriminator pedestal and width for 64 channels. From data in Figure 11. Note that the FULL width of the pedestal spread is 12 ADC counts (excluding the first channels that have a pick up from digital lines), equivalent to 0.75 photo-electrons. TriP 1 and 2, MCM IIb, Module 0.

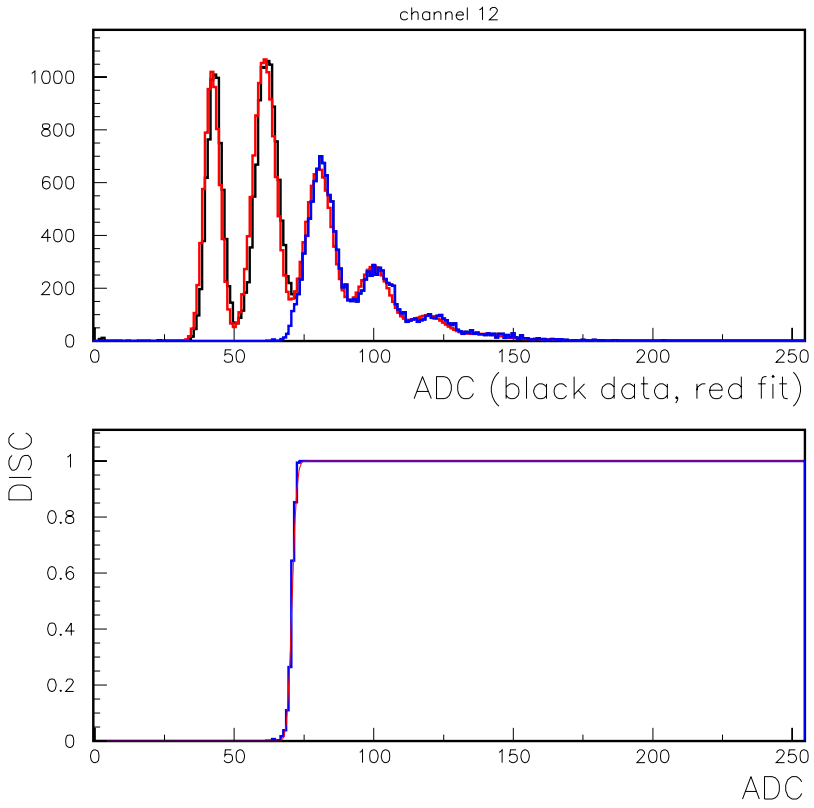

Figure 13: Histogram of ADC for all events and for events with discriminator fired (upper plot) and their ratio. Also shown in the upper plot is the fit used to extract pedestal, gain, noise and mean number of photo-electrons. Channel 12, TriP 1, MCM IIb, Module 1.

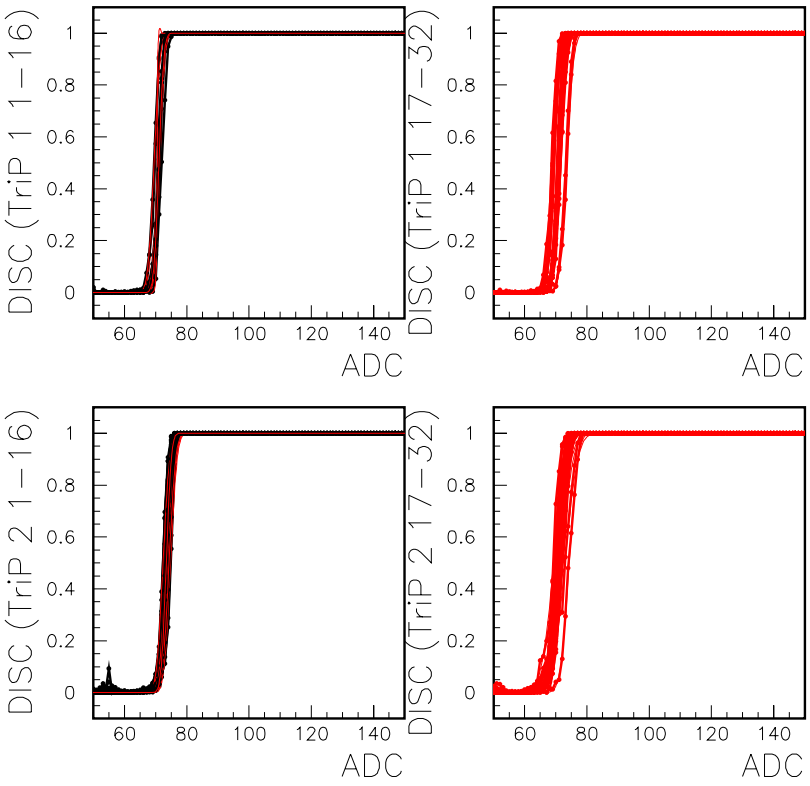

Figure 14: Discriminator turn-on curves for 64 channels as a function of ADC (as lower plot of Figure 13). TriP 1 and 2, MCM IIb, Module 1.

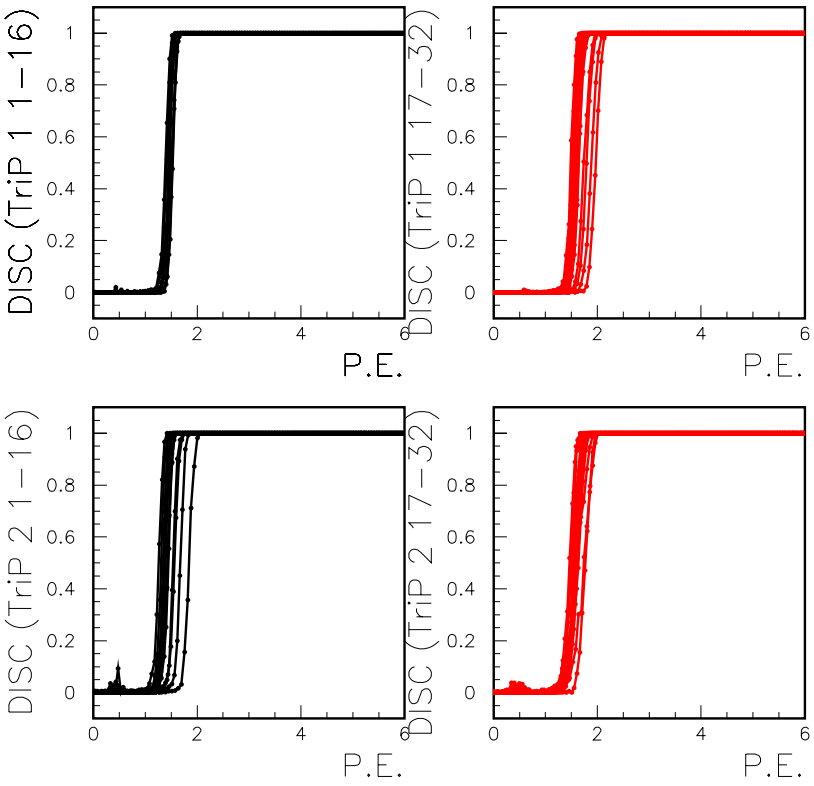

Figure 15: Discriminator turn-on curves for 64 channels as a function of the number of photo-electrons obtained from the fit. TriP 1 and 2, MCM IIb, Module 1.

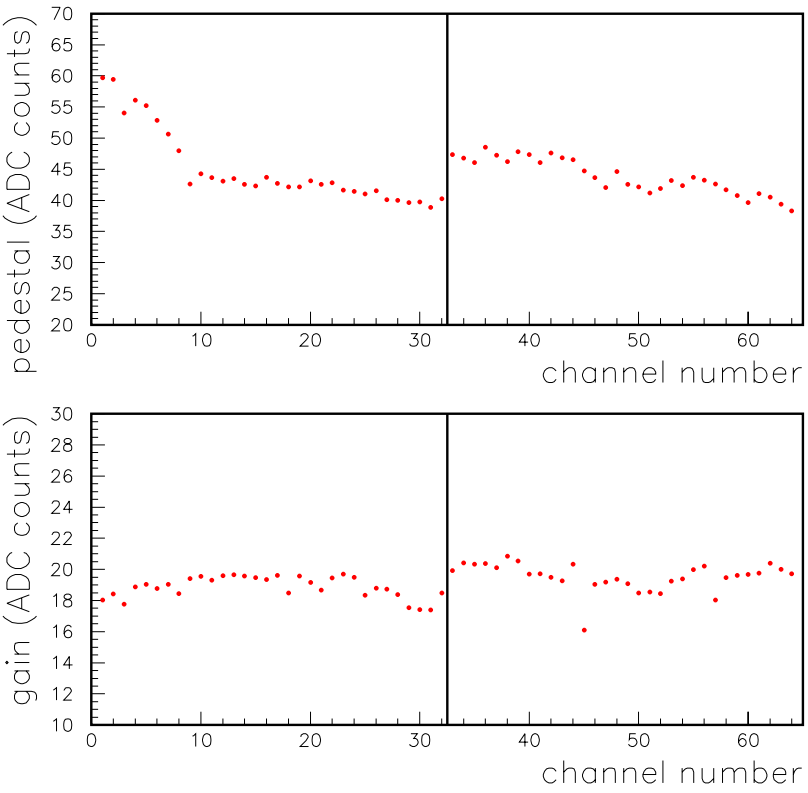

Figure 16: Pedestal and gain for 64 channels. TriP 1 and 2, MCM IIb, Module 1.The high pedestal of channels 1 to 8 of TriP 1 is due to cross-talk between digital clocks and analog inputs, which should be absent in AFE II, see the text.

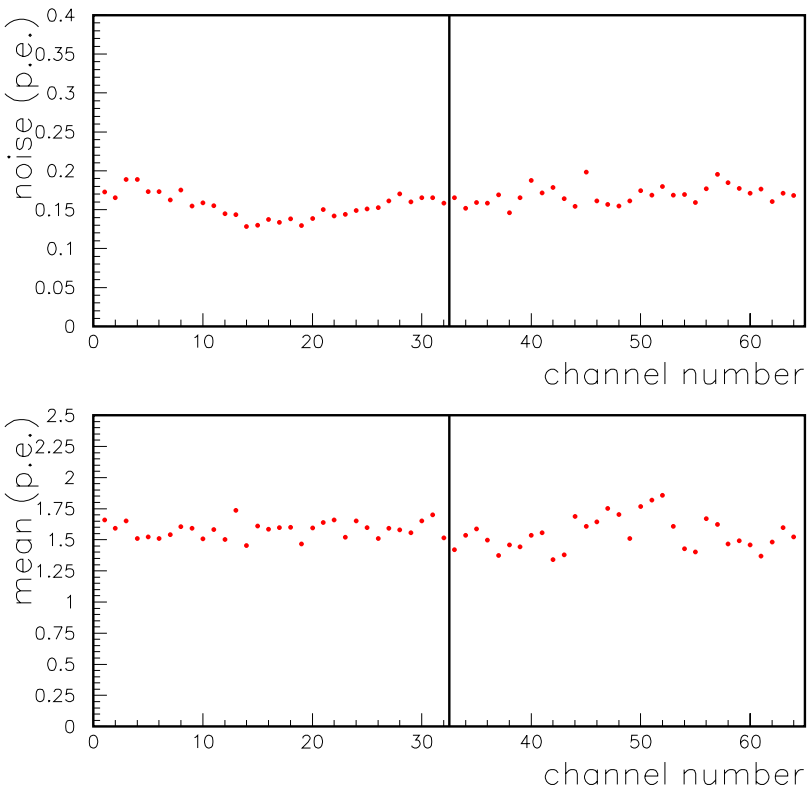

Figure 17: Noise (one standard deviation) and mean number of photo-electrons for 64 channels. TriP 1 and 2, MCM IIb, Module 1.

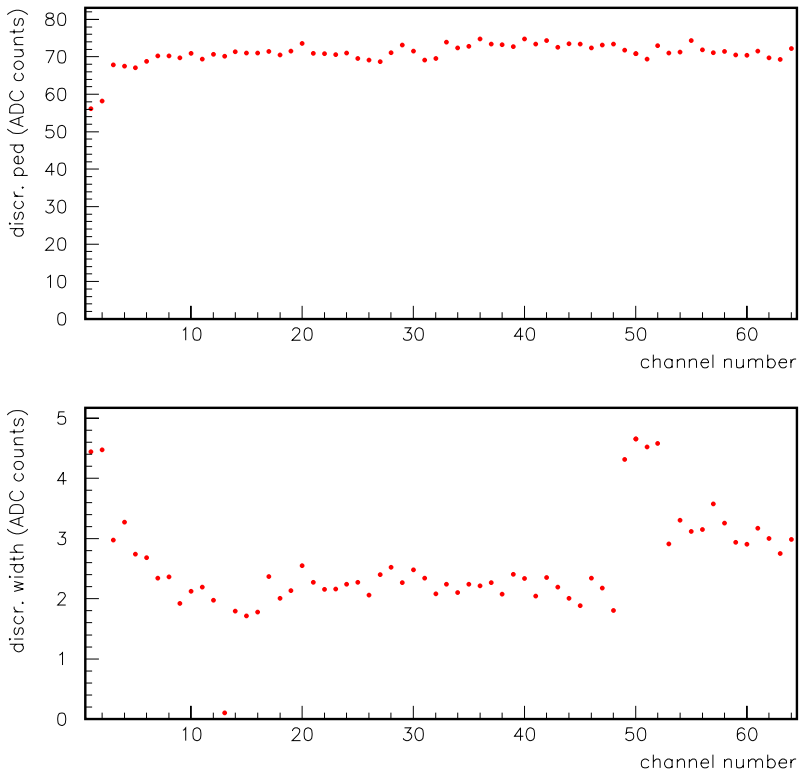

Figure 18: Discriminator pedestal (at which it fires 50% of the time) and discriminator width (1 standard deviation) for 64 channels. TriP 1 and 2, MCM IIb, Module 1. The discriminator width is half the interval from 16% firing to 84% firing as determined by the fitted error function.

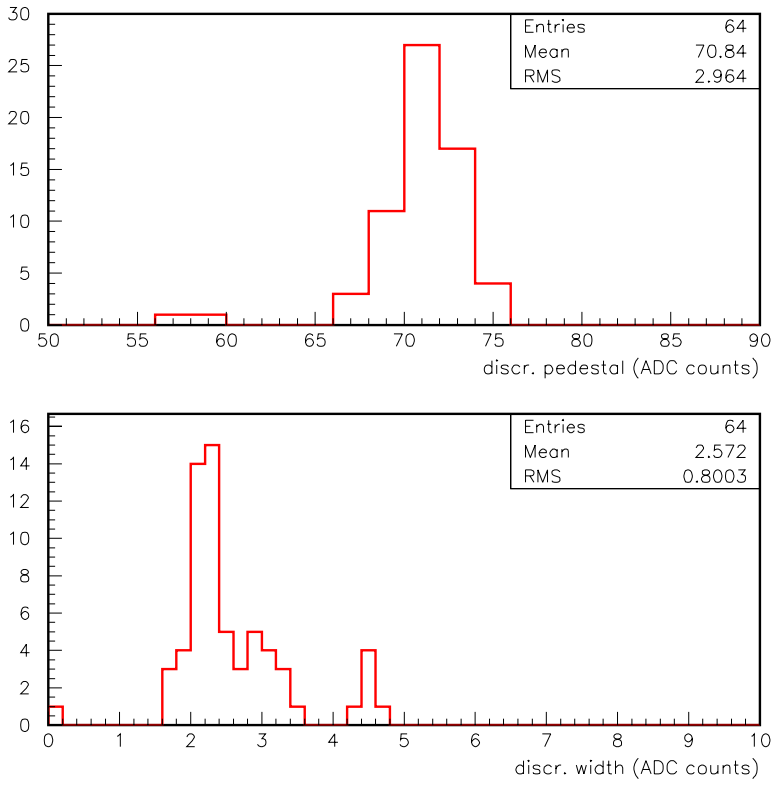

Figure 19: Histogram of discriminator pedestal and width for 64 channels. From data in Figure 18. Note that the FULL width of the pedestal spread is 10 ADC counts (excluding the first channels that have pickup from digital lines) equivalent to 0.5 photo-electrons. TriP 1 and 2, MCM IIb, Module 1.

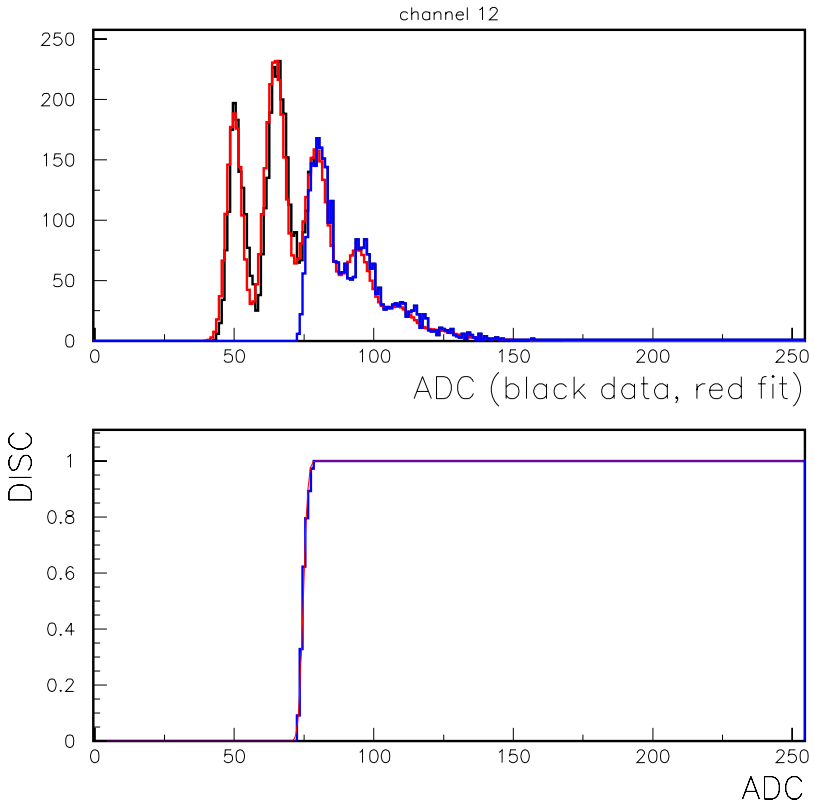

Figure 20: Histogram of ADC for all events and for events with discriminator fired (upper plot) and their ratio (lower plot). Also shown in the upper plot is the fit used to extract pedestal, gain, noise and mean number of photo-electrons. Channel 12, TriP 2, MCM IIb, Module 2.

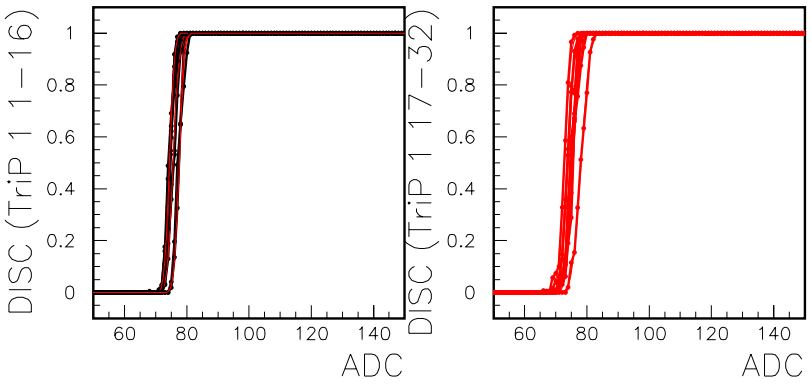

Figure 21: Discriminator turn-on curves for 32 channels as a function of ADC (as lower plot of Figure 20). TriP 2, MCM IIb, Module 2.

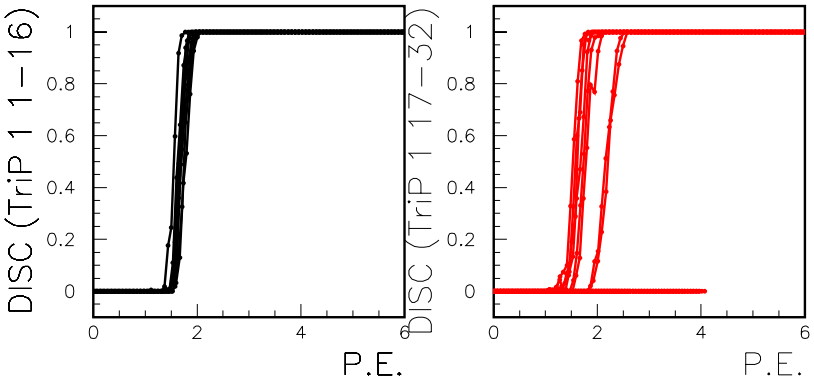

Figure 22: Discriminator turn-on curves for 32 channels as a function of the number of photo-electrons obtained from the fit. The fit did not converge for some channels even tho the spectra looks OK. TriP 2, MCM IIb, Module 2.

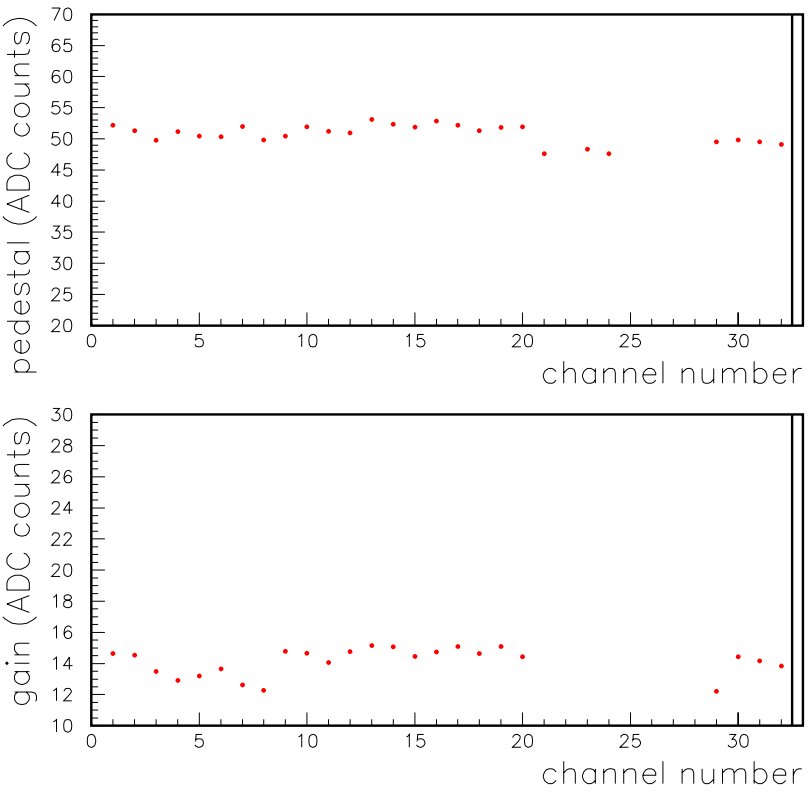

Figure 23: Pedestal and gain for 32 channels. TriP 2, MCM IIb, Module 2. Some channels on this AFE board have no bias on the VLPC.

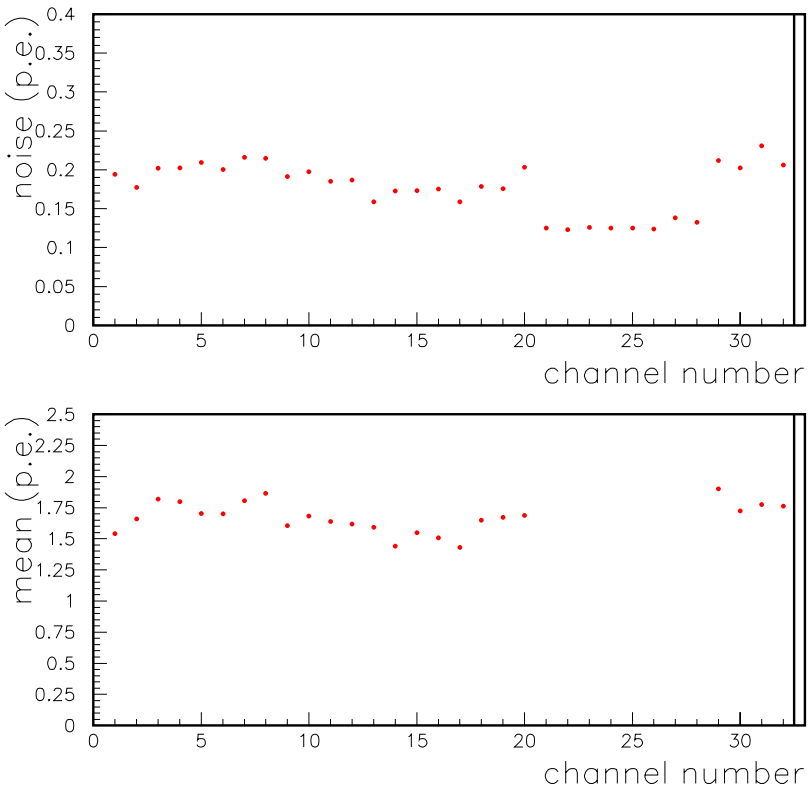

Figure 24: Noise (one standard deviation) and mean number of photo-electrons for 32 channels. TriP 2, MCM IIb, Module 2. Some channels on this AFE board have no bias on the VLPC.

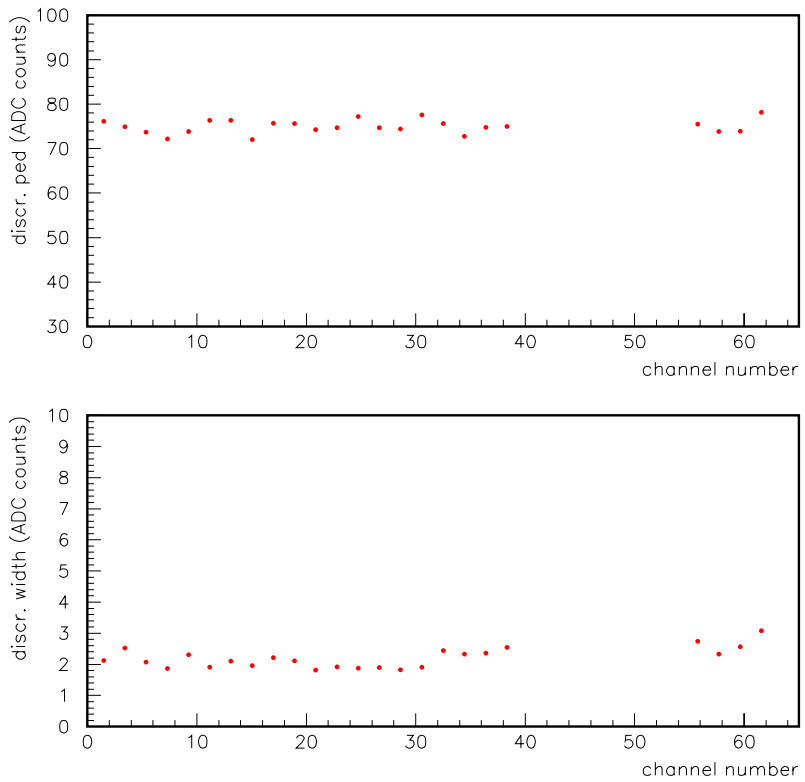

Figure 25: Discriminator pedestal (at which it fires 50% of the time) and discriminator width (1 standard deviation) for 32 channels Some channels on this AFE board have no bias on the VLPC. channels. TriP 2, MCM IIb, Module 2. The discriminator width is half the interval from 16% firing to 84% firing as determined by the fitted error function. Some channels on this AFE board have no bias on the VLPC.

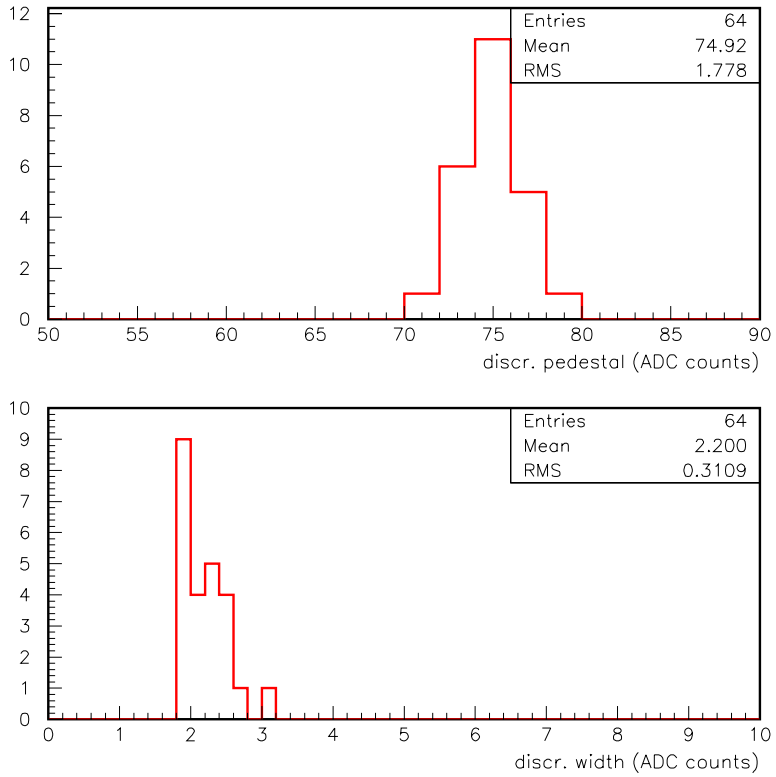

Figure 26: Histogram of discriminator pedestal and width for 32 channels. Note that the FULL width of the pedestal spread is 10 ADC counts or 0.7 photo-electrons. TriP 2, MCM IIb, Module 2.

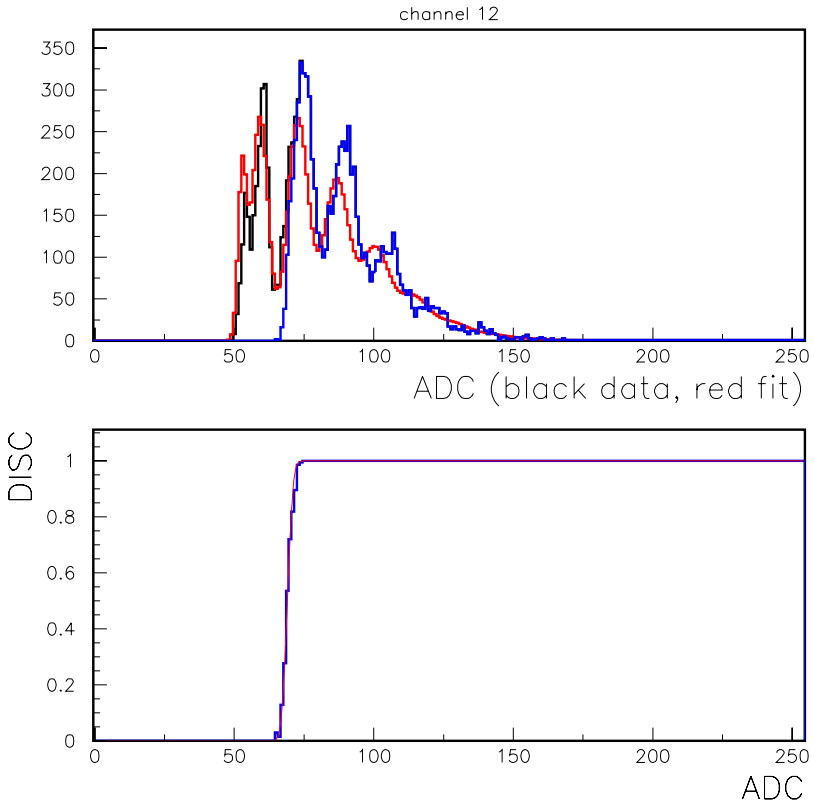

Figure 27: Histogram of ADC for all events and for events with discriminator fired (upper plot) and their ratio (lower plot). Also shown in the upper plot is the fit used to extract pedestal, gain, noise and mean number of photo-electrons. Some channels, such as this one, have poor fits. Channel 12, MCM IIc, Module 3. Encapsulated TriP chip.

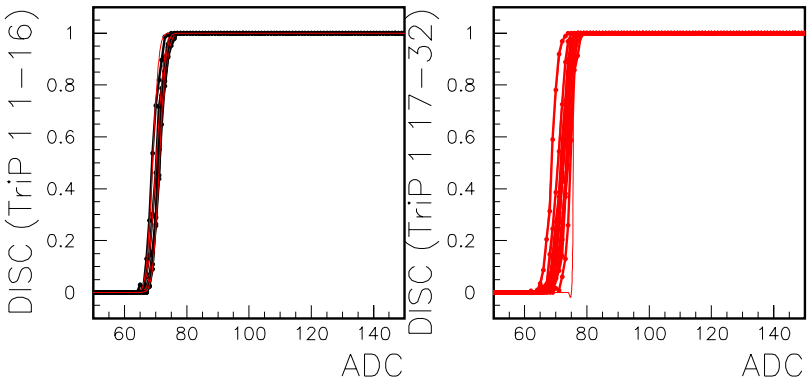

Figure 28: Discriminator turn-on curves for 32 channels as a function of ADC (as lower plot of Figure 27). MCM IIc, Module 3.

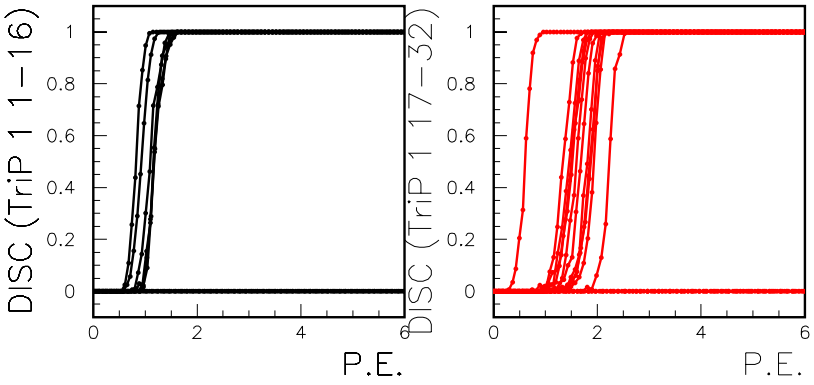

Figure 29: Discriminator turn-on curves for 32 channels as a function of the number of photo-electrons obtained from the fit. Some channels have poor fits and some VLPC's have no bias. MCM IIc, Module 3.

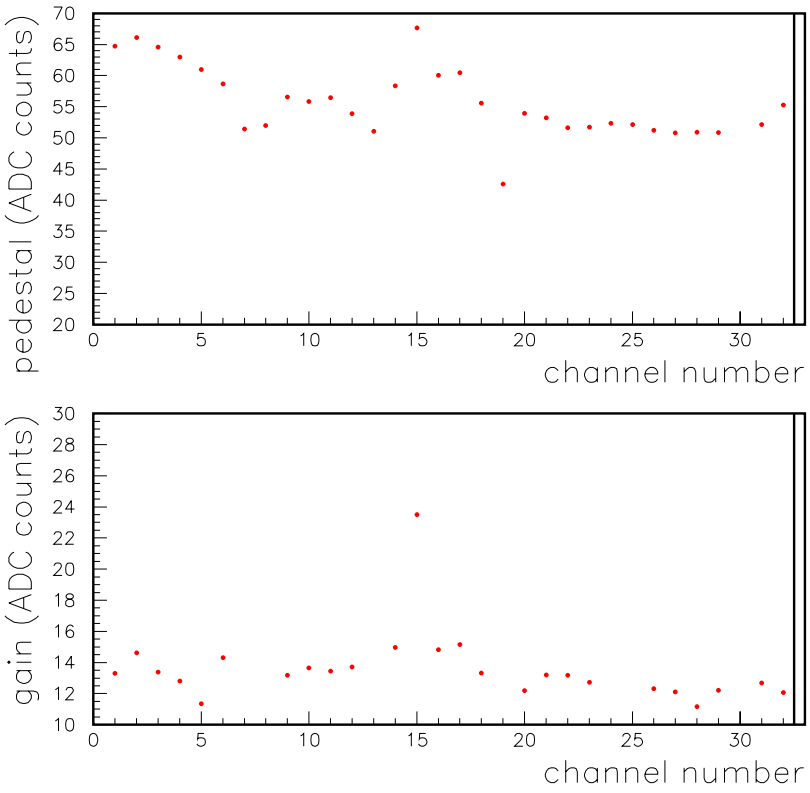

Figure 30: Pedestal and gain for 32 channels. MCM IIc, Module 3.

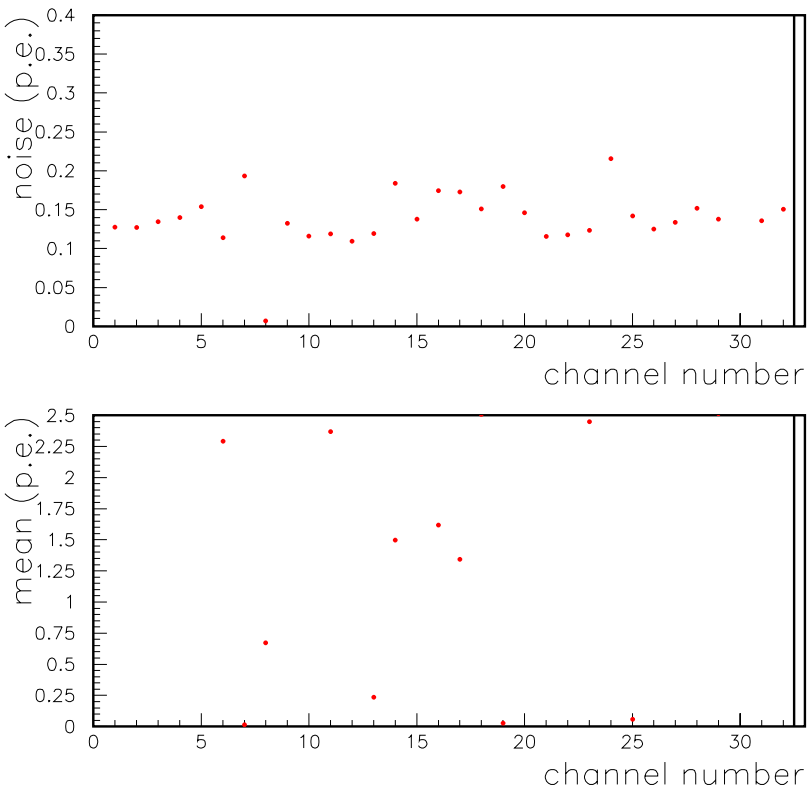

Figure 31: Noise (one standard deviation) and mean number of photo-electrons for 32 channels. MCM IIc, Module 3. Some fits are poor.

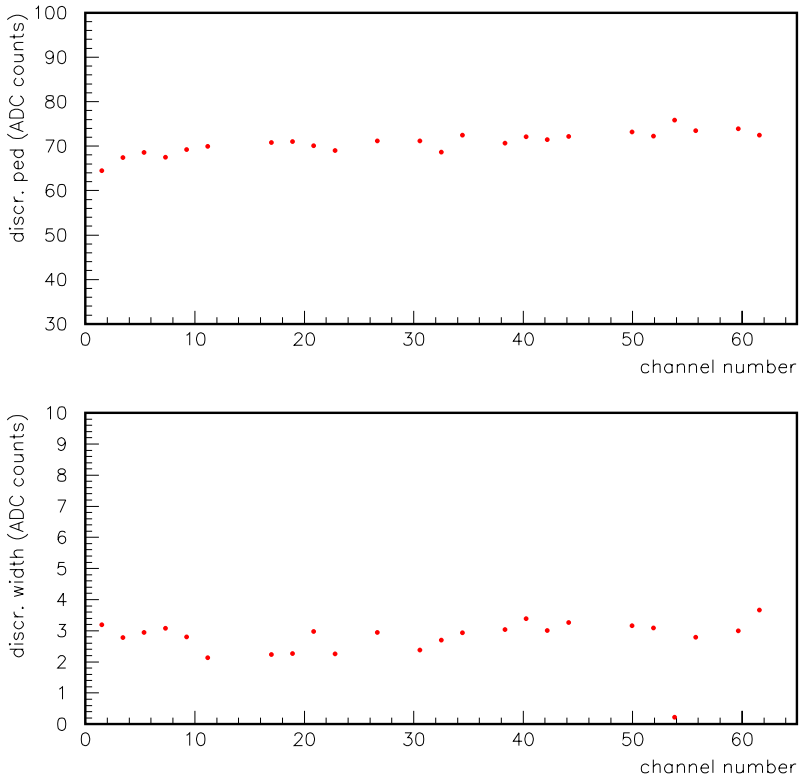

Figure 32: Discriminator pedestal (at which it fires 50% of the time) and discriminator width (1 standard deviation) for 32 channels. MCM IIc, Module 3. The discriminator width is half the interval from 16% firing to 84% firing as determined by the fitted error function.

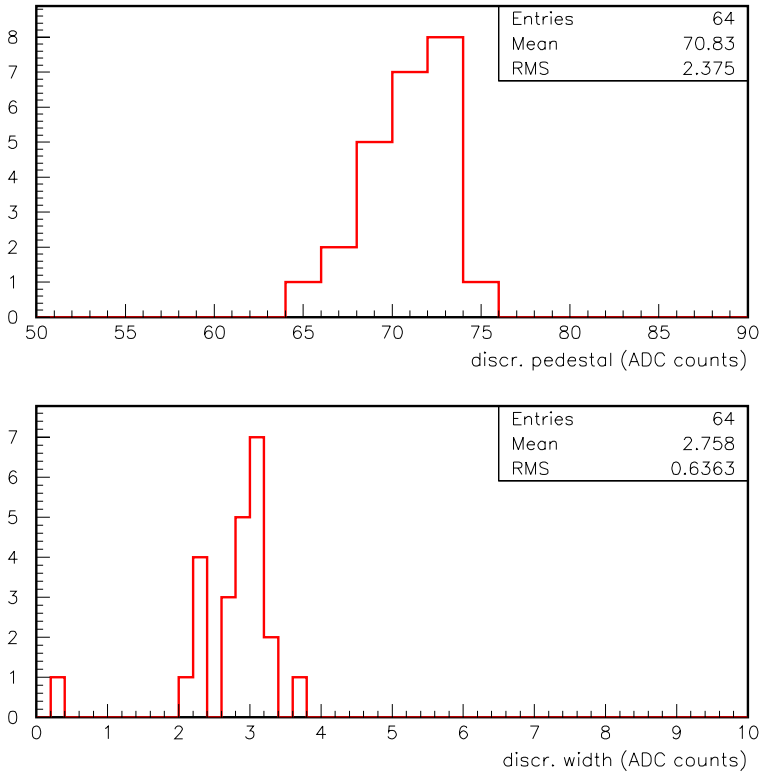

Figure 33: Histogram of discriminator pedestal and width for 32 channels. Note that the FULL spread of the pedestal is 12 ADC counts, equivalent to 0.86 photo-electrons. MCM IIc, Module 3.

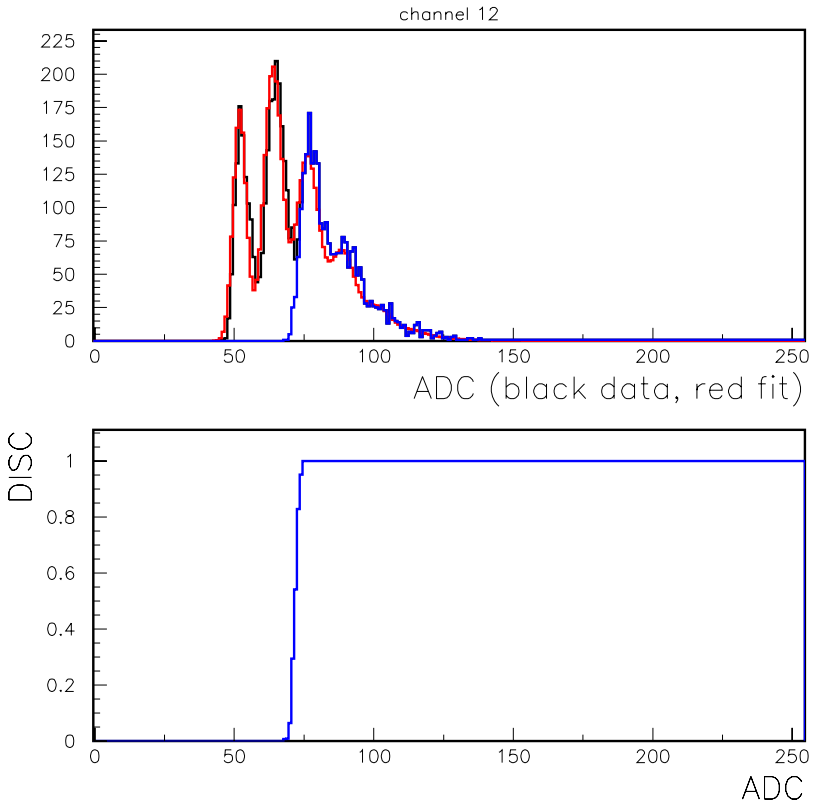

Figure 34: Histogram of ADC for all events and for events with discriminator fired (upper plot) and their ratio. Also shown in the upper plot is the fit used to extract pedestal, gain, noise and mean number of photo-electrons. Channel 12, MCM IIc, Module 5.

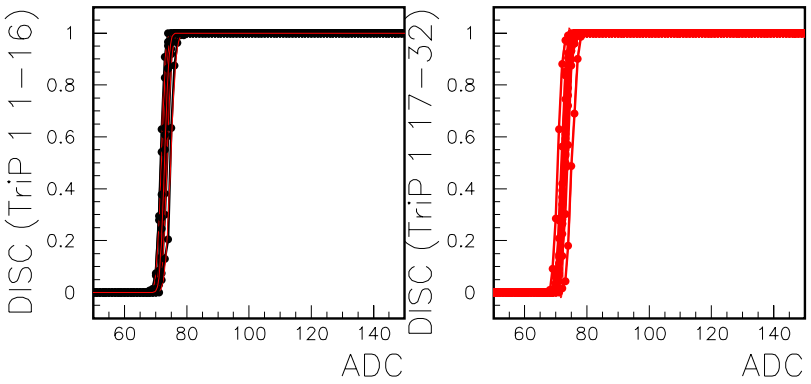

Figure 35: Discriminator turn-on curves for 32 channels as a function of ADC (as lower plot of Figure 34). MCM IIc, Module 5.

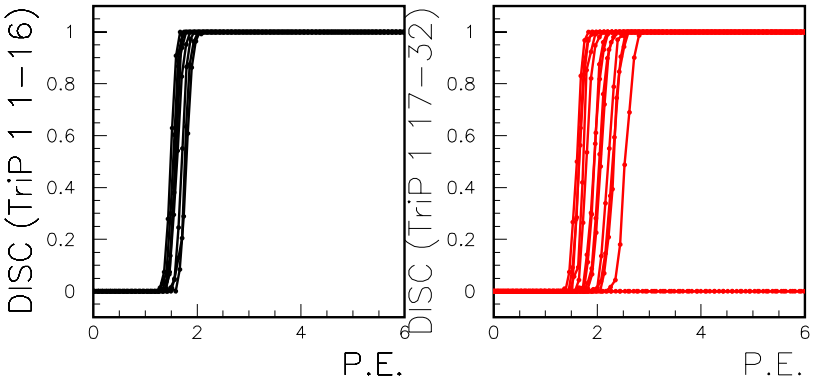

Figure 36: Discriminator turn-on curves for 32 channels as a function of the number of photo-electrons obtained from the fit. Some channels have no VLPC bias. MCM IIc, Module 5.

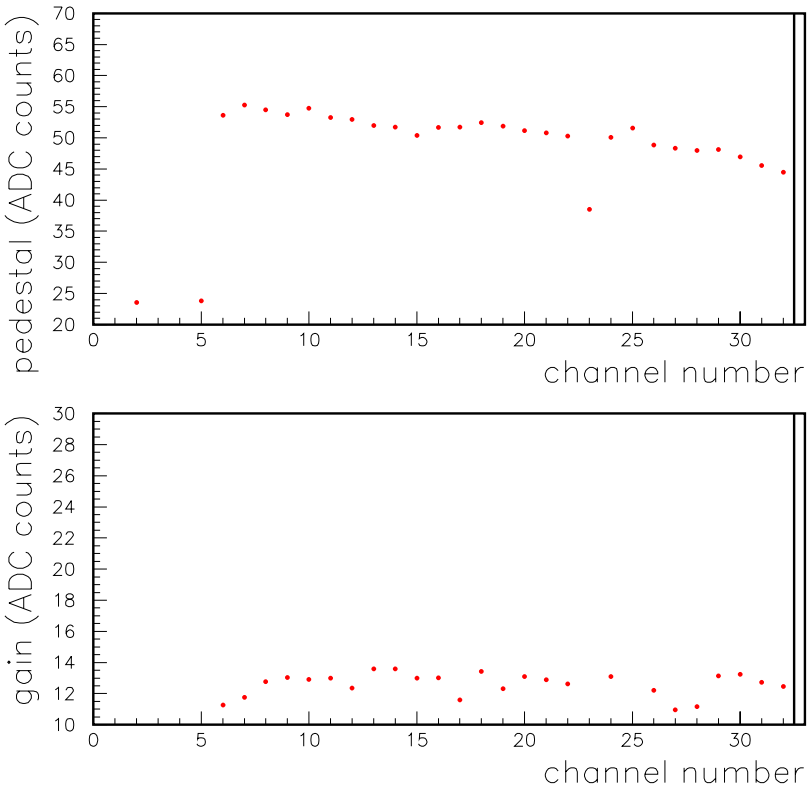

Figure 37: Pedestal and gain for 32 channels. MCM IIc, Module 5.

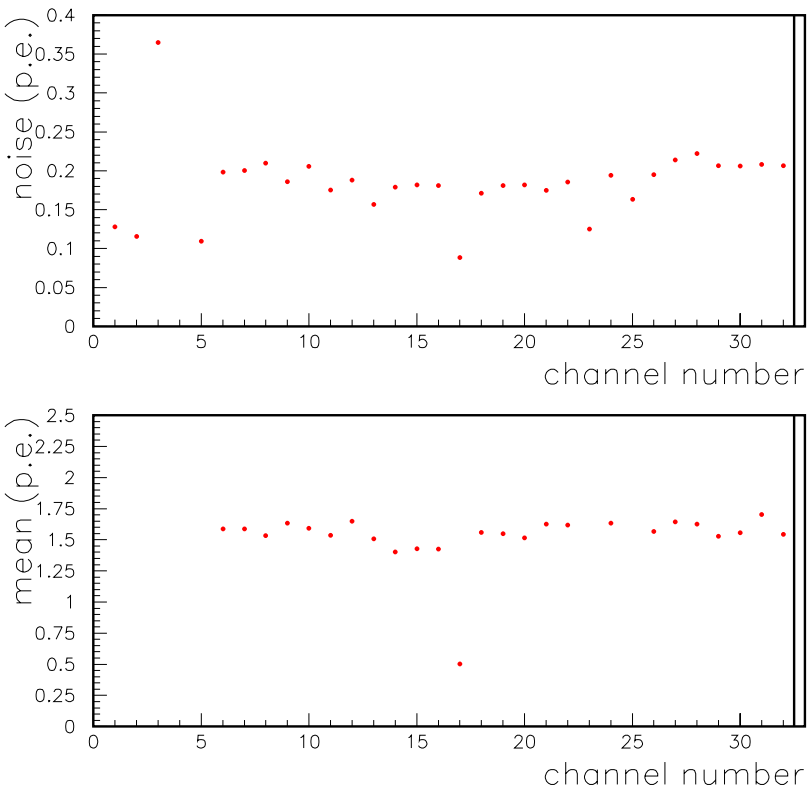

Figure 38: Noise (one standard deviation) and mean number of photo-electrons for 32 channels. MCM IIc, Module 5.

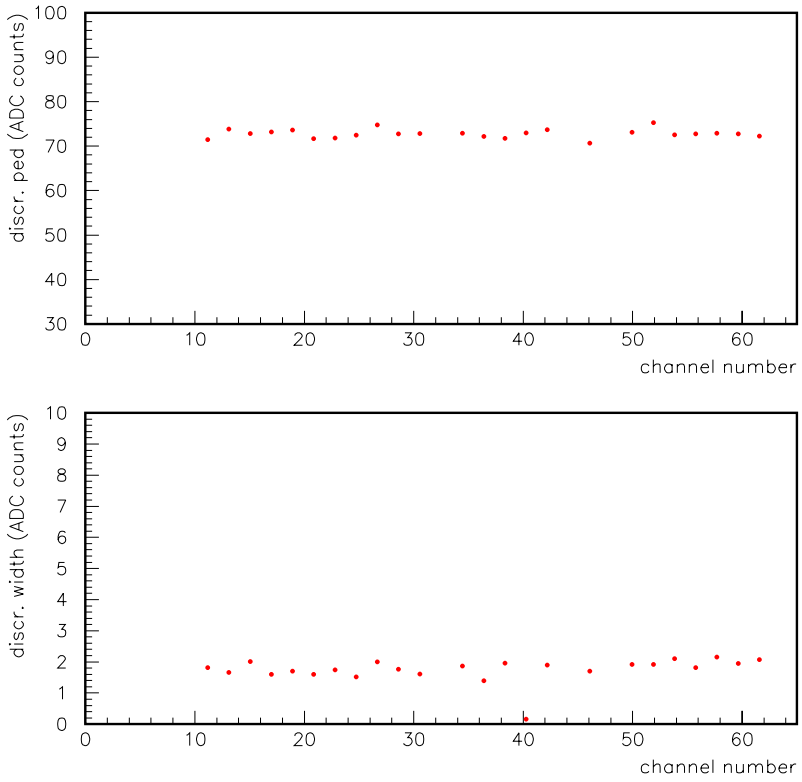

Figure 39: Discriminator pedestal (at which it fires 50% of the time) and discriminator width (1 standard deviation) for 32 channels. MCM IIc, Module 5. The discriminator width is half the interval from 16% firing to 84% firing as determined by the fitted error function.

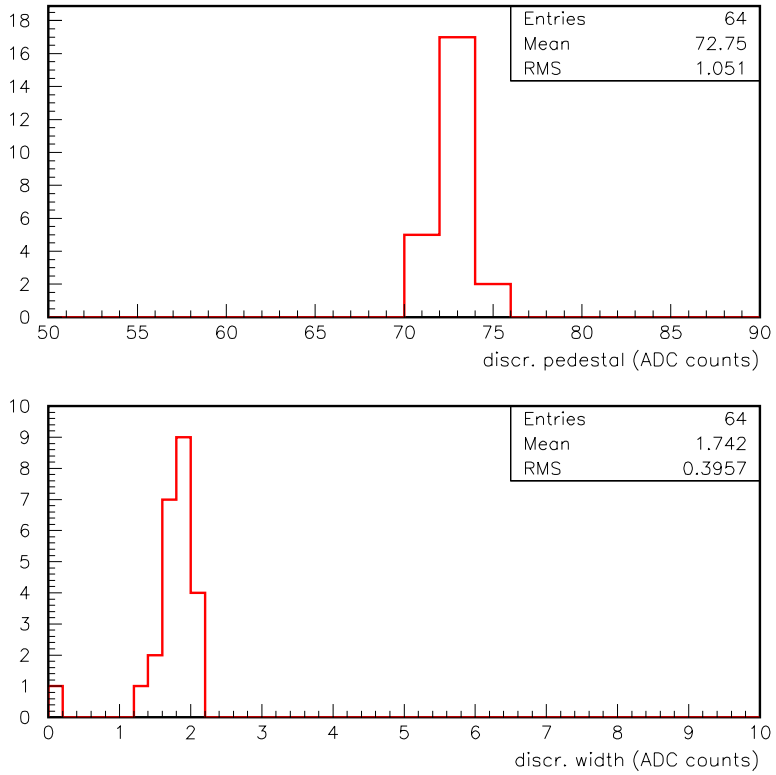

Figure 40: Histogram of discriminator pedestal and width for 32 channels. Note that the FULL spread of the pedestal is 6 ADC counts, equivalent to 0.5 photo-electrons. MCM IIc, Module 5.

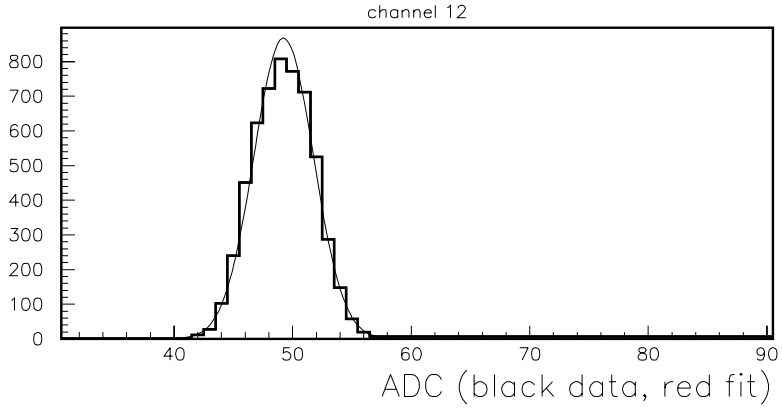

Figure 41: Histogram of ADC with no light and no VLPC bias. Window of integration is $\tau = 82.5$ns. The high pedestal of the first few channels is due to pick up from digital lines, see the text. Channel 12, TriP's 1 and 2, module 1.

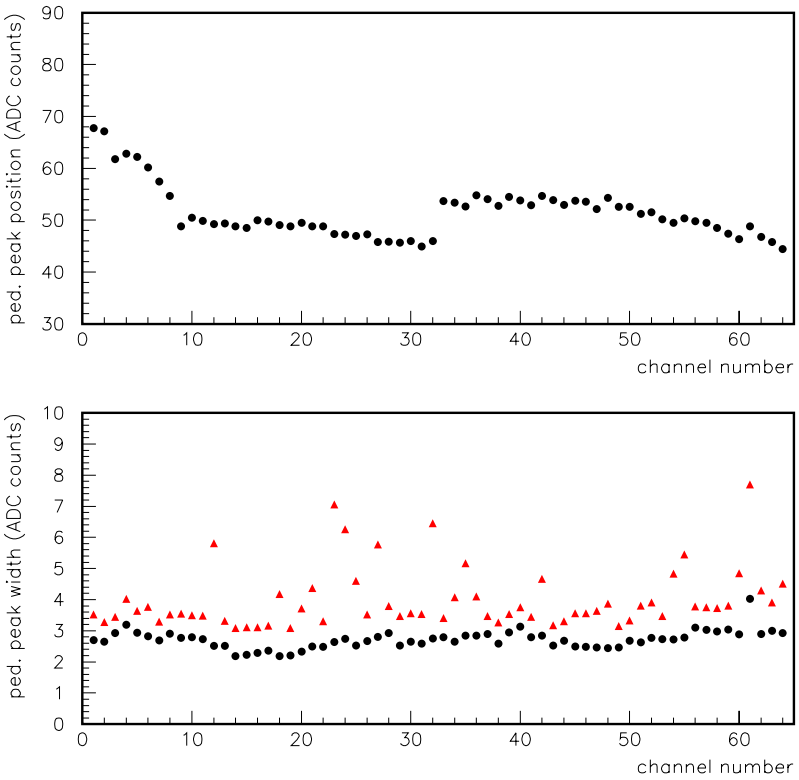

Figure 42: Peak and width of the fit to the ADC counts with no light and no VLPC bias. The rms width and the 1 standard deviation of the gaussian fit are shown. The window of integration is $\tau = 82.5$ns. 64 channels of TriP's 1 and 2, module 1.

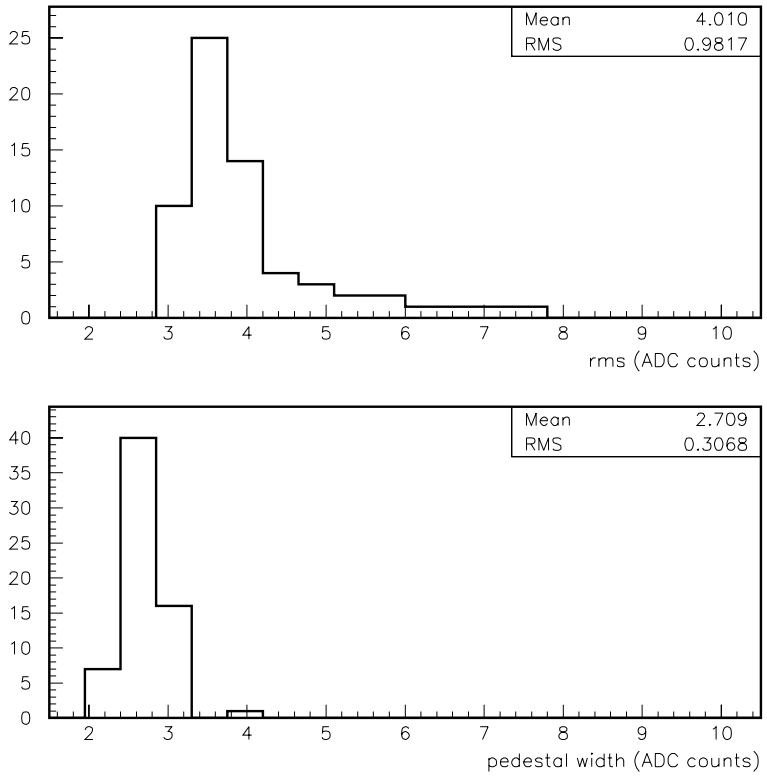

Figure 43: Histogram of noise with no light and no VLPC bias. Upper plot: rms; lower plot: 1 standard deviation from gaussian fit. From data in Figure 42. The window of integration is $\tau = 82.5$ns. 64 channels of TriP's 1 and 2, module 1.

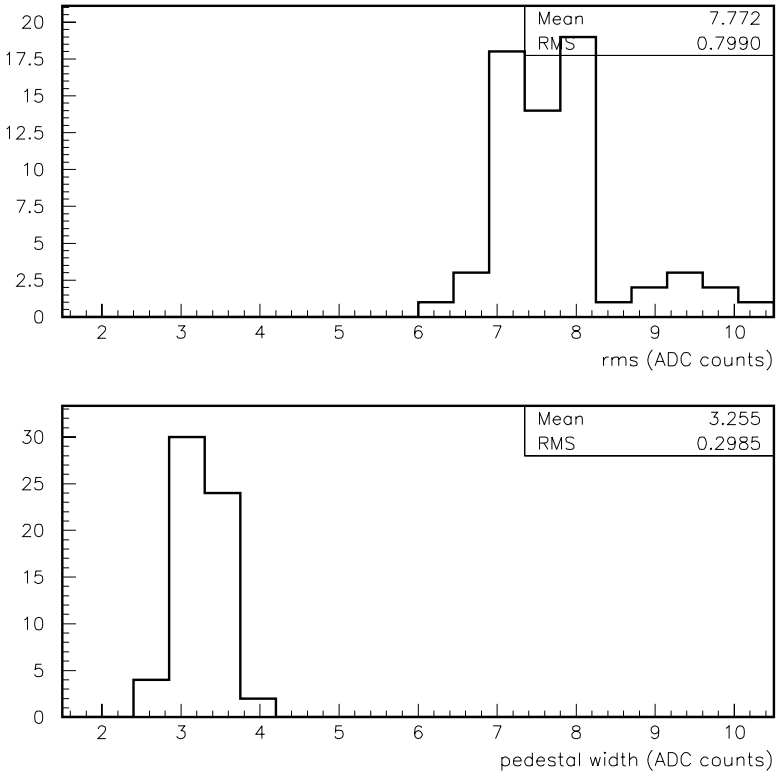

Figure 44: Histogram of noise with no light and with VLPC bias. Upper plot: rms; lower plot: 1 standard deviation from gaussian fit. From data in Figure 42. The window of integration is $\tau = 82.5$ns. 64 channels of TriP's 1 and 2, module 1.

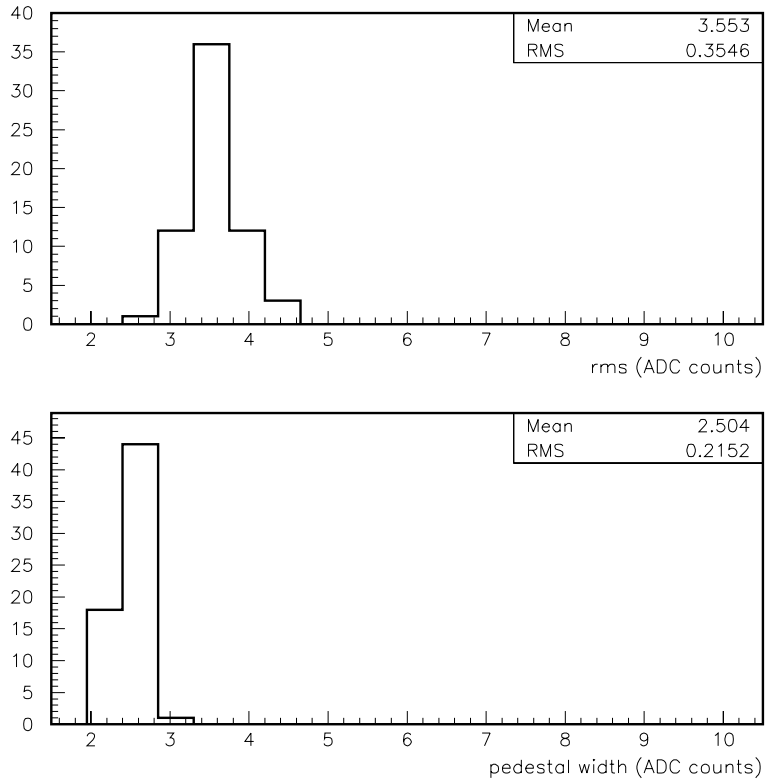

Figure 45: Histogram of noise with no light and no VLPC bias. Upper plot: rms; lower plot: 1 standard deviation from gaussian fit. The window of integration is $\tau = 57.75$ns. 64 channels of TriP's 1 and 2, module 1.

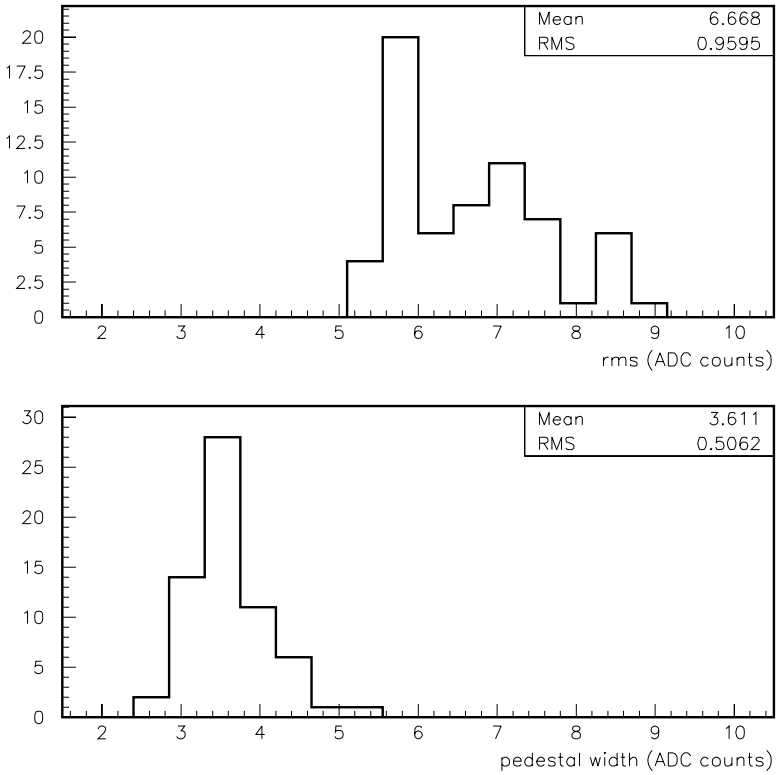

Figure 46: Histogram of noise with no light and with VLPC bias. Upper plot: rms; lower plot: 1 standard deviation from gaussian fit. The window of integration is $\tau = 57.75$ns. 64 channels of TriP's 1 and 2, module 1.

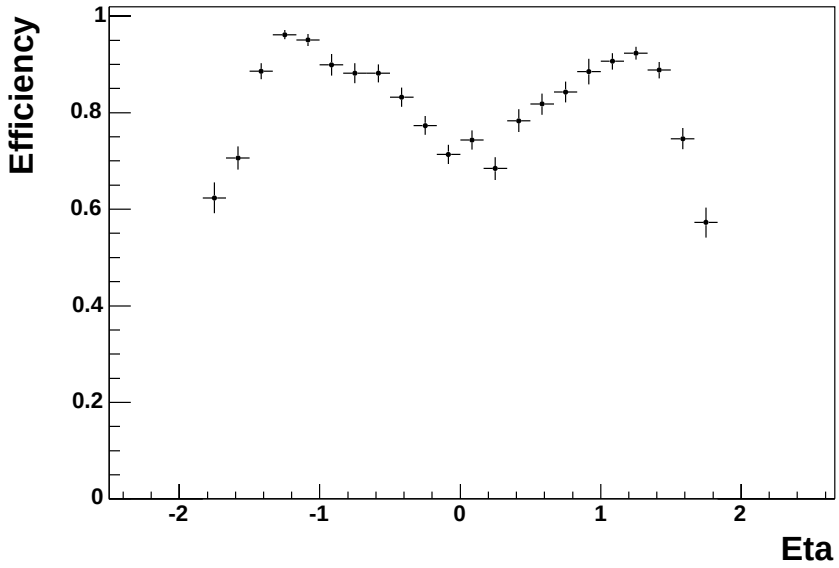

Figure 47: Reco tracking efficiency as a function of η for isolated muons from $Z \rightarrow \mu^+\mu^-$. The drop in efficiency near $\eta = 0$ is due to lower light yield for normal incidence. Figure provided by Emily Nurse, August 2003.[8] Reco version p13.